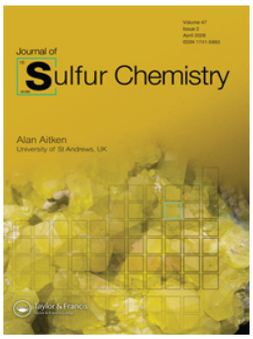

Journal of Sulfur Chemistry

ISSN: 1741-5993 (Print) 1741-6000 (Online) Journal homepage: www.tandfonline.com/journals/gsrp20

Computational investigation of the oxidation reactions of S_3 and S_4 with O_2

Nadia Sebbar , Henning Bockhorn & Dimosthenis Trimis

To cite this article: Nadia Sebbar , Henning Bockhorn & Dimosthenis Trimis (24 Apr 2026): Computational investigation of the oxidation reactions of S_3 and S_4 with O_2, Journal of Sulfur Chemistry, DOI: 10.1080/17415993.2026.2659134

To link to this article: https://doi.org/10.1080/17415993.2026.2659134

JOURNAL OF SULFUR CHEMISTRY
https://doi.org/10.1080/17415993.2026.2659134

Computational investigation of the oxidation reactions of S_3 and S_4 with O_2

Nadia Sebbar, Henning Bockhorn and Dimosthenis Trimis

Engler-Bunte Institut/ Verbrennungstechnik, Karlsruhe Institut für Technologie, Karlsruhe, Germany

ABSTRACT

In this work, the reaction pathways and products resulting from the reactions $^1S_3 + {}^3O_2$ and $^1S_4 + {}^3O_2$ are investigated using three different quantum chemistry methods. The thermochemistry of formation, isomerization and degradation reactions for all species involved in these systems is evaluated in detail and the corresponding reaction profiles, including reactants, transition states, and products, are reported. Enthalpies are calculated at the CBS-QB3, G3, G4 levels of theory. Entropy and heat capacity contributions as functions of temperature are determined from the optimized molecular structures, moments of inertia and vibrational frequencies. Kinetic parameters are obtained using canonical transition state theory (TST) calculations. All reaction pathways in both systems ultimately lead to ^1S_2O, ^3SO, ^3S, $^3S_2$, and $^1SO_2$ as final products. The calculations indicate that analogous reaction types in the two systems exhibit similar rate coefficients.

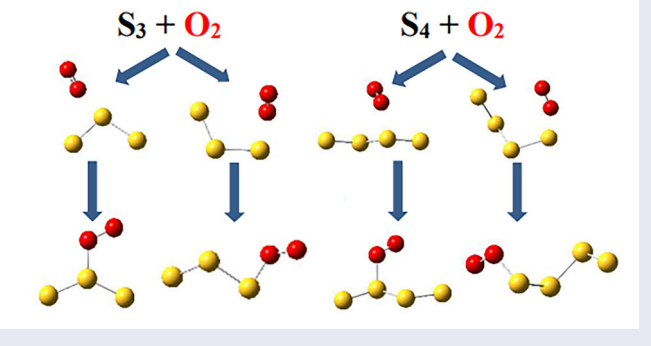

ARTICLE HISTORY
Received 29 January 2026
Accepted 1 April 2026

KEYWORDS
Sulfur combustion; Oxidation; Thermochemistry; S_3O_2; S_4O_2

CONTACT Nadia Sebbar nadia.sebbar@partner.kit.edu Engler-Bunte Institut/ Verbrennungstechnik, Karlsruhe Institut für Technologie, Engler-Bunte-Ring 7, Karlsruhe 76131, Germany

Supplemental data for this article can be accessed online at https://doi.org/10.1080/17415993.2026.2659134.

1. Introduction

Sulfur, the 16th most abundant element in the lithosphere, is widely available and easy to store, which has made solid sulfur a common feedstock in industrial processes for decades. Among its various applications, the production of sulfuric acid is particularly significant, as it remains one of the highest-volume industrial chemicals worldwide. In conventional sulfuric acid plants, elemental sulfur is combusted on a large scale, with the released heat primarily used for steam and/or electricity generation.

The industrial sulfuric acid production process potentially can be modified for utilizing energy from renewable sources. One concept suggests thermal energy from sunlight [1] which is integrated via a closed energy cycle involving sulfur as energy carrier. By this, a portion of the produced sulfuric acid is thermally split into SO_2 and H_2O and O_2 followed by the recovery of elemental sulfur via the disproportionation of SO_2 into elemental sulfur, O_2 and sulfuric acid. The heat of reaction for the endothermic decomposition of H_2SO_4 is supplied by solar energy. Depending on the demand for sulfuric acid and the availability of solar energy, the overall process can be shifted from conventional sulfuric acid production toward partial or complete sulfur recycling via sulfuric acid decomposition within a closed energy conversion cycle. The integration of solar energy utilizes solid particles as a heat transfer medium, enabling the storage of solar energy both as thermal energy and as chemical energy in solid sulfur. A detailed description of a process based on this concept of a closed energy conversion process enabling to generate electricity continuously around the clock with energy from a solar-powered plant is provided in [2]. In this process, the key reaction step is the combustion of elemental sulfur.

Combustion of elemental sulfur requires high-performance plants that are designed and optimized based on validated reaction mechanisms. Since research on sulfur combustion has been primarily motivated by the widely applied Claus process, most reaction mechanisms available in the literature focus on sulfur compound reactions coupled with hydrocarbon or hydrogen combustion see e.g. references [3–8]. Only a limited number of studies address the oxidation of sulfur in the absence of hydrogen or hydrocarbons. Therefore, the objective of the present study is to contribute to the development of a detailed combustion mechanism and to evaluate the corresponding reaction rate coefficients for sulfur oxidation under hydrogen- and hydrocarbon-free conditions.

In the following paragraphs studies on the oxidation of sulfur in the absence of hydrogen or hydrocarbons from the existing literature are discussed and its main findings related to the topic are outlined. Du et al. [9] found that recombination of S atoms occurs stepwise from elemental S atoms to the most abundant molecule S_8. They report that the scarcely investigated reaction $S + S_2 \rightarrow S_3$ could be a key intermediate step in the formation of sulfur aerosols in low-O_2 atmospheres. The kinetics of this reaction are reported with Ar used as the chaperone molecule in the production of S_3 via two complex intermediates: $SAr + S_2$ and $S_2Ar + S$. Francisco [10] examined the mass-dependent and non-mass-dependent fractionations of elemental sulfur isotopes to exploit the nature of the sulfur cycle in the atmosphere. Interpretation of the experimental data required the estimation of the energetics of the reaction $S + S_2 \rightarrow S_3$, which is isoelectronic with $O + O_2 \rightarrow O_3$. Key molecular properties of the S potential-energy surface, such as vibrational frequencies and isotopic shifts, were reported. Ab initio results were compared with the available experimental results for S_2 to evaluate the reliability of the computational results for S_3.

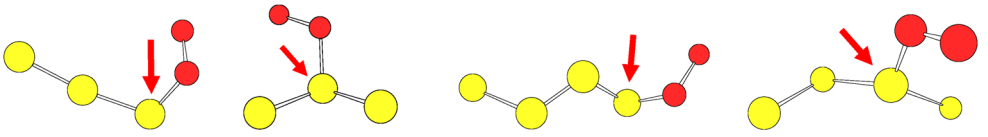

Figure 1. Addition of O_2 on terminal and inner sulfur of $^1S_3$ and $^1S_4$.

Matus et al. [11] reported ab initio electronic structure calculations for S_4. Geometric and energetic parameters were calculated using single and double coupled-cluster methods. The calculated geometry for the ground state singlet structure of S_4 is in good agreement with the microwave structure determined for S_4. Wong and Steudel [12] investigated the structures and relative stabilities of eight S_4 isomers by G3X(MP2), CCSD(T)/cc-pVTZ and MRCI/CASSCF calculations. The cis-planar structure is confirmed to be the global minimum of S_4. McCarthy et al. [13] observed the rotational spectrum of S_4 for the first time in an electrical discharge through sulfur vapor.

It is well established that gaseous sulfur exists in a variety of molecular forms, S_x, with x ranging from 1 to 8. Each of these species can react with oxygen to generate multiple intermediates, which are subsequentially converted to the stable products SO_2 and SO_3. In a series of previous studies, components of a detailed combustion mechanism were developed. The starting point was a basic mechanism [14], which represents a slightly modified version of a mechanism derived from the work of Glarborg et al. [15]. This basic set was subsequently extended to include singlet and triplet species, as well as cis- and trans-adducts formed through the reaction of O_2 with S_2 [16]. Subsequent studies treated the formation/decomposition of S_1 to S_8 species under oxygen-free conditions [17] and the oxidation of these species via attack of O_2 at the terminal sulfur atoms, followed by decomposition of the primary oxidation products [18]. The present work extends this investigation to the detailed investigation of oxidation reactions occurring in the systems $^1S_3 + {}^3O_2$ and $^1S_4 + {}^3O_2$, considering O_2 attack of at both terminal and non-terminal S. These systems serve as representative models for understanding how O_2 may interact with terminal and non-terminal sulfur atoms in larger species, S_5 to S_8. Several studies have addressed the formation of S_3 and S_4; however, to the best of our knowledge, no oxidation reactions of S_3 and S_4 have been reported in the literature.

In the following, the addition of O_2 to S_x ($x = 3, 4$) leading to formation of a peroxy radical ($S_x + O_2 \rightarrow S_xO_2$) is investigated. The resulting peroxy radicals can subsequently undergo various addition and decomposition reactions through multiple competing pathways. For both systems, S_3 and S_4, two reactive sites are accessible for O_2 addition. O_2 can either add to the terminal sulfur atom or to the inner (non-terminal) sulfur atom, as illustrated in Figure 1.

In this article spin multiplicity of atoms and compounds are indicated whenever appropriate and necessary. If multiplicity is omitted, the notation comprises the predominantly existing electron spin configurations.

2. Computational methods

Estimation of the energies of compounds resulting from the addition of $^3O_2$ on $^1S_3$ and $^1S_4$ are obtained with the help of the Gaussian 16 program suite [19]. Results of previous studies [14,16] brought about that the ab-initio methods CBS-QB3 [20], G3 [21], and G4 [22] are suitable for the determination of the thermodynamic and kinetic properties of the systems under consideration. CBS-QB3 uses the B3LYP level for the calculation of the structures and zero-point vibrational energies. In the Gaussian-4 (G4) method, the QCISD(T) approach is replaced by CCSD(T) for the highest level of correlation treatment. In addition, two new higher-level corrections are added to try and account for deficiencies in the energy calculations.

In the previous study [16] and in order to check the reliability and accuracy of the methodology, the heat of reaction $\Delta_r H^0_{298}$ was calculated for the reactions $^3S_2 + {}^3O_2 \rightarrow 2\ {}^3SO$ and $^3S_2 + {}^3O_2 \rightarrow {}^3S + {}^1SO_2$ using the literature values of $^3S_2$, $^3O_2$, ^3SO and $^1SO_2$. The values were compared with the results obtained with CBS-QB3, G3B3, G4 and W1U [23] and showed a good agreement among literature data and the calculations. For the reaction $S_2 + O_2 \rightarrow 2SO$, the literature reaction enthalpy is -28.34 kcal mol^{-1}, compared to -27.07, -29.28, and -28.54 kcal mol^{-1} obtained with CBS-QB3, G3, and G4, respectively. Similarly, for the reaction $S_2 + O_2 \rightarrow S + SO_2$, the reaction enthalpy derived from literature data is -35.43 kcal mol^{-1}, whereas values of -33.21, -33.75, and -35.0 kcal mol^{-1} were obtained using CBS-QB3, G3, and G4, respectively. Furthermore, Ref. [16] reports a systematic comparison of eight sulfur species with literature data from Goodarzi et al. [24], demonstrating agreement within 2–3 kcal mol^{-1}.

Entropies and heat capacities $Cp(T)$ are calculated for all species (adducts, S^0_{298} intermediates, products and transition state structures) involved in the investigated systems $S_3/S_4 + O_2$. The structures of each compound are illustrated in Table 1, Table 2, Table 3 and Table 4. All thermodynamic data are listed in the supplementary material which includes also optimized geometries, frequencies and moments of inertia. Entropy and heat capacity calculations are based on the vibration frequencies and moments of inertia obtained from the selected optimized structures using the SMCPS code [25] based on formulas from statistical mechanics.

3. Results

3.1. Enthalpies of formation

3.1.1. The $^1S_3 + {}^3O_2$ system

3.1.1.1. Attack of O_2 at terminal sulfur atom of S_3. Standard enthalpies of formation for compounds involved in the reaction system $^3S_3 + {}^3O_2$ along with the illustration of their structures are reported in Table 1. Standard enthalpies of formation for ^1SOO [14], ^3S, $^3S_2$ [26], ^3SO, $^1SO_2$, and ^1SSO [27] used as reference in the work reactions are taken from the literature.

Using the three methods of computation, optimized geometries of the different species and transition state structures resulting from the addition of O_2 on the terminal sulfur of S_3 were evaluated. For most of the species, the results show agreement across the three applied methods, within 3–4 kcal mol^{-1} for calculated energies which is considered as very

Table 1. Attack of O_2 at the terminal sulfur atom of S_3. Standard enthalpy of formation for species ($\Delta_f H^0_{298}$) and transition state structures (ΔH_{TS}) involved in the $^1S_3 + {}^3O_2$ reaction system calculated at CBS-QB3, G3 and G4 levels in kcal mol^{-1}, Y means cyclic.

Structure	Reactions for $\Delta_f H^0_{298}$ and ΔH_{TS} calculation	$\Delta_f H^0_{298}$ in kcal mol^{-1}		
		CBS-QB3	G3	G4
Reference data: ^3S: 66.24; $^3S_2$: 30.74; ^3SO: 1.2; $^1SO_2$: -70.94; ^1S_2O: -13.5; ^3O: 58; ^1SOO: 45.8				
Addition of O_2 on terminal Sulfur atom of S_3				
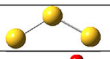	$^1S_3$-linear Ref. 28 = **33.8**	34.3	34.8	**34.0**
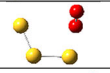	$^1S_3 + {}^3O_2 \rightarrow$ **^{3}TSA** $\rightarrow {}^1S_3O_2$	60.5	**60.6**	61.6
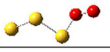	**$^1S_3O_2$**	53.2	50.6	**50.5**
Channel-1				
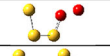	$^1S_3O_2 \rightarrow$ **^{3}TS1** $\rightarrow S_3O + O$	**71.5**	77.1	73.6
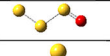	**^1S_3O**	**8.2**	9.8	9.0
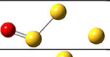	$^1S_3O \rightarrow$ **^{1}TS1-1** $\rightarrow {}^3S + {}^1SSO$	37.3	35.5	**38.9**
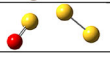	$^1S_3O \rightarrow$ **^{3}TS1-2** $\rightarrow {}^3S_2 + {}^3SO$	15.8	**15.9**	16.8
Channel-2				
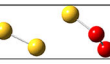	$^1S_3O_2 \rightarrow$ **^{3}TS2** $\rightarrow {}^3S_2 + {}^1SOO$	60.6	**61.6**	76.9
Channel-3				
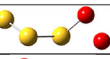	$^1S_3O_2 \rightarrow$ **^{1}TS3** $\rightarrow {}^3S_2SO_2$	-	**71.3**	94.2
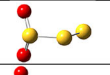	**$^3S_2SO_2$**	-8.0	**-8.0**	-7.4
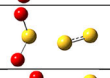	$^3S_2SO_2 \rightarrow$ **^{3}TS3-1** $\rightarrow {}^3S_2 + {}^1SO_2$	-10.2	**-8.5**	-4.5
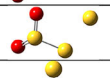	$^3S_2SO_2 \rightarrow$ **^{3}TS3-2** $\rightarrow {}^3S + {}^1SSO_2$	**14.0**	14.6	16.2
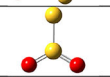	**$^1SSO_2$** [Ref. 16]	-42.7	**-41.9**	-43.3
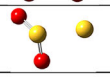	$^1SSO_2 \rightarrow$ **^{1}TS3-3** $\rightarrow {}^3S + {}^1SO_2$	13.2	**11.5**	12.9

(*continued*).

good agreement among methods, particularly for sulfur-containing species where electron correlation effects may be significant. Observed differences in calculated enthalpies can be attributed to variations in the geometries. Values selected for further analysis were chosen based on careful examination of the geometries; in cases of similar geometries, the structure with the lowest calculated energy was favored. Based on these criteria, the recommended values for the enthalpies of formation are highlighted in bold in Table 1. The attack of triplet oxygen ($^3O_2$) at the terminal sulfur atom of S_3 results in the formation of a peroxy radical, S_3O_2. This intermediate subsequently undergoes bond cleavage and rearrangement processes through six distinct reaction pathways, leading to the formation of several different compounds. As mentioned above, good agreement can be stated

Table 1. Continued.

Channel-4				
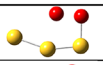	$^1S_3O_2 \rightarrow {}^1$**TS4** $\rightarrow {}^3SYS_2O_2$	**99.0**	126.4	99.1
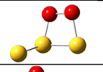	**$^1SYS_2O_2$**	66.8	68.6	**66.0**
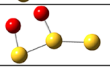	$^3SYS_2O_2 \rightarrow {}^3$**TS4-1** $\rightarrow {}^1$SSOSO	**92.2**	105.0	96.3
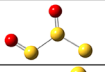	**^{1}SSOSO**	**-2.7**	-0.8	-1.3
	^{1}SSOSO $\rightarrow {}^1$**TS4-2** $\rightarrow {}^1$SSO + SO	10.7	**13.2**	9.1
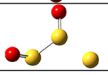	^{1}SSOSO $\rightarrow {}^3$**TS4-3** $\rightarrow {}^1$OSSO + ^{3}S cis-OSSO: -30.44 at G3 level [Ref. 16]	20.7	**20.6**	20.9
Channel-5				
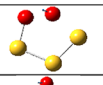	$^1S_3O_2 \rightarrow {}^3$**TS5A** $\rightarrow {}^1YS_3O_2$	-	**91.1**	-
	$^1S_3O_2 \rightarrow {}^3$**TS5B** $\rightarrow {}^3OS_3O$	**75.7**	-	75.5
	**$^1YS_3O_2$**	31.4	32.2	**30.9**
	$^1YS_3O_2 \rightarrow {}^1$**TS5-1** $\rightarrow {}^3$OS3O	32.4	**29.5**	33.7
	**$^3OS_3O$**	-19.4	-19.0	**-18.5**
	$^3OS_3O \rightarrow {}^1$**TS5-2** $\rightarrow {}^1$SSO + ^{3}SO	-16.6	**-15.6**	-13.7
	$^1YS_3O_2 \rightarrow {}^1$**TS5-3** $\rightarrow {}^1$SSO + ^{3}SO	-	**49.8**	-
Channel-6				
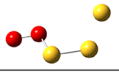	$^1S_3O_2 \rightarrow {}^3$**TS6** $\rightarrow {}^1S_2O_2 + {}^3S$ $^1S_2O_2$: 35.99 at G3 level [Ref. 16]	72.0	**72.5**	72.9

among the three applied computational methods. The G3 calculation for the (**TS1**) transition state associated with O-O bond scission in S_3O_2 shows a deviation of approximately 6 kcal mol^{-1} relative to the selected value obtained at the CBS-QB3 level. This discrepancy can be attributed to differences in the optimized geometries of the transition state.

Structural analysis indicates that the G3-optimized geometry exhibits a different SS–SO dihedral angle compared with the CBS-QB3 and G4 structures. As illustrated in Figure 2, the G3 geometry yields a nearly planar arrangement with a dihedral of 0.17°, whereas the CBS-QB3 ang G4 optimization gives a slightly twisted structure with a dihedral of 7.58° and 6.35°, respectively. As shown in Table 1 such variations in transition-state geometry can significantly influence the calculated activation energy. Notably, the CBS-QB3 and G4 geometries are comparable and lead to similar enthalpy values, whereas the G3 optimization results in a slightly higher energy.

The calculated energy of the **TS3** transition state for the *ipso* addition of oxygen at the G3 level is 71.3 kcal mol^{-1}, which is significantly lower than the value obtained using G4

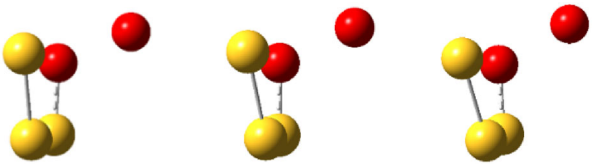

Figure 2. Illustration of the transition state structure **TS1** from G3 calculations (left) and CBS-QB3 (middle) and G4 calculations (right).

optimization (94.2 kcal mol^{-1}). This discrepancy can be attributed to differences in the optimized geometries, particularly the (S1–S2–S3–O4) dihedral angle obtained from the two methods. The G3-optimized structure exhibits a dihedral angle of 117.32°, whereas the G4-optimized geometry yields a larger value of 157.16°, as illustrated in Figure 3. These geometric differences likely influence the steric interactions in the transition state, thereby affecting the calculated activation energy.

The enthalpies calculated for (**TS4**) at the CBS-QB3 and G3 levels also exhibit a substantial deviation, which can be explained by differences in the final optimized geometries. Frequency analysis of the G3 transition-state structure indicates a displacement of sulfur (S2) nearly parallel to oxygen (O4), with an S2–S1–O3–O4 dihedral angle of 33.5°. This motion can be interpreted as an umbrella-type vibration involving the S5–S2–S1 framework. In contrast, the CBS-QB3-optimized geometry shows a distinct displacement of O4 toward S2 and is characterized by an almost perfectly planar S2–S1–O3–O4 dihedral angle of 0.008° (see Figure 4). These pronounced geometric differences in the transition-state structures account for the observed variation in the calculated enthalpies. The enthalpy calculated at the G4 level is not shown in Figure 4 because the optimized structure and dihedral angles are identical to those obtained at the CBS-QB3 level. Moreover, the resulting energy values are very similar, with 99.1 kcal mol^{-1} for G4 compared to 99.0 kcal mol^{-1} for CBS-QB3.

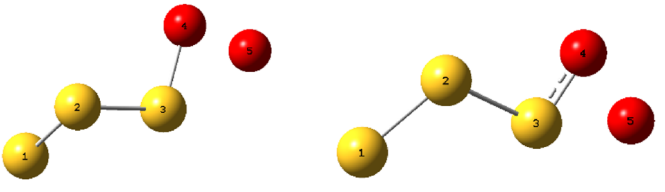

Figure 3. Illustration of the transition state structure **TS3** from G3 calculations (left) and G4 calculations (right).

The energy calculated at the G3 level for the transition state structure associated with ring formation of $^{1}Y(S_3O_2)$, **TS5A**, deviates significantly from the values obtained with the other two methods, see Table 1. Analysis of the vibrational frequencies reveals that the CBS-QB3 and G4 calculations correspond to a different transition state than that identified at the G3 level.

For CBS-QB3 and G4, the imaginary frequency shows a O – O bond scission (**TS5B**) rather than ring closure requiring less energy than cyclization and explaining the discrepancies of the calculated energy barriers among the methods

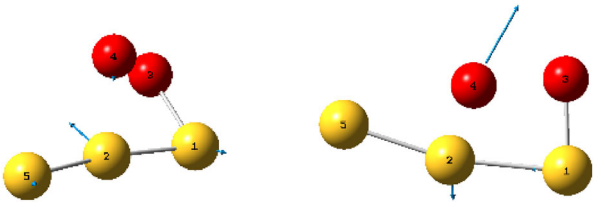

Figure 4. Illustration of the transition state structure **TS4** from G3 calculations (left) and CBS-QB3 calculations (right).

Table 2. Attack of O_2 at the central sulfur atom of S_3. Standard enthalpy of formation for species ($\Delta_f H^0_{298}$) and transition state structures (ΔH_{TS}) involved in the $^1S_3 + {}^3O_2$ reaction system calculated at CBS-QB3, G3 and G4 levels in kcal mol^{-1}, Y means cyclic.

Structure	Reactions for $\Delta_f H^0_{298}$ and ΔH_{TS} calculation	$\Delta_f H^0_{298}$ in kcal mol^{-1}		
		CBS-QB3	G3	G4
Reference data: ^3S: 66.24; $^3S_2$: 30.74; ^3SO: 1.2; $^1SO_2$: -70.94; ^1SSO: -13.5; ^3O: 58; ^1SOO: 45.8				
Addition of O_2 on the central sulfur atom of S_3				
	$^1S_3 + {}^3O_2 \rightarrow$ **^{3}TSB-a** $\rightarrow {}^1$iso-S_3O_2	83.8	**94.4**	91.0
	**iso-$^1S_3O_2$**	**69.5**	72.1	73.5
	$^1S_3 + {}^3O_2 \rightarrow$ **^{3}TSB-b** $\rightarrow {}^1S_2O_2 + {}^3S$	90.4	**101.3**	102.3
Channel-1				
	^{1}iso-$S_3O_2 \rightarrow {}^3$**TS1** $\rightarrow {}^1$iso-$S_3O + {}^3O$	**96.6**	98.7	98.9
	**iso-^1S_3O**	11.0	11.8	**10.4**
	$^1iS_3O \rightarrow {}^1$**TS1-1** $\rightarrow {}^3S + {}^1SSO$	58.4	**43.3**	59.6
Channel-2				
	^{1}iso-$S_3O_2 \rightarrow {}^3$**TS2** $\rightarrow {}^3SYS_2O_2$ See continuation in Table 1 and Fig. 9	102.4	**104.8**	107.6
Channel-3				
	^{1}iso-$S_3O_2 \rightarrow {}^1$**TS3** $\rightarrow {}^1SYSO_2S$	103.2	**103.9**	104.7
	**$^1SYSO_2S$**	51.5	**50.6**	50.4
	$^1SYSO_2S \rightarrow {}^3$**TS3-1** $\rightarrow {}^3S + SSO_2$	97.9	**100.2**	97.2
Channel-4				
	^{1}iso-$S_3O_2 \rightarrow {}^1$**TS4** $\rightarrow {}^1S_2O_2 + {}^3S$ S_2O_2: 35.99 at G3 level [Ref. 16]	106.3	97.0	**101.5**

Table 3. Attack of O_2 at the terminal sulfur atom of S_4. Standard enthalpy of formation ($\Delta_f H^0_{298}$) and transition state structures (ΔH_{TS}) resulting from species involved in the $^1S_4 + {}^3O_2$ system calculated at CBS-QB3, G3 and G4 levels in kcal mol^{-1}, Y means cyclic.

Structure	Reactions for $\Delta_f H^0_{298}$ and ΔH_{TS} calculation	$\Delta_f H^0_{298}$ in kcal mol^{-1}		
		CBS-QB3	G3	G4
Reference data: ^3S: 66.24; $^3S_2$: 30.74; ^3SO: 1.2; $^1SO_2$: -70.94; ^1S_2O: -13.5; ^3O: 58; ^1SOO: 45.8				
Addition of O_2 on terminal sulfur atom of S_4				
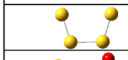	$^1S_4$: **34.87** [28]	33.8	39.6	35.6
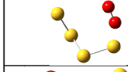	$^1S_4$-linear + $^3O_2 \rightarrow$ **^{3}TSA** $\rightarrow$ $^3S_4O_2$	73.5	**70.9**	71.8
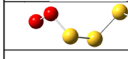	**$^3S_4O_2$**	**52.1**	54.7	53.3
Channel-1				
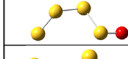	$^3S_4O_2 \rightarrow$ **^{3}TS1** $\rightarrow$ $^3S_4O + {}^3O$	79.0	**79.3**	79.9
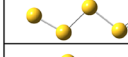	**^3S_4O**	**19.4**	21.9	20.6
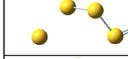	$^3S_4O \rightarrow$ **^{3}TS1-1** $\rightarrow$ $^3S + {}^1S_3O$	41.7	**43.7**	43.8
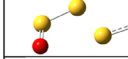	$^3S_4O \rightarrow$ **^{3}TS1-2** $\rightarrow$ $^3S_2 + {}^1S_2O$	17.1	20.8	**21.9**
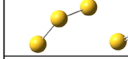	$^3S_4O \rightarrow$ **^{3}TS1-3** $\rightarrow$ $^1S_3 + {}^3SO$	**42.4**	43.9	43.8
Channel-2				
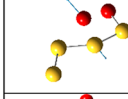	$^3S_4O_2 \rightarrow$ **^{1}TS2** $\rightarrow$ $^1S_2SOSO$	91.2	**102.1**	90.4
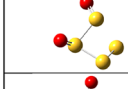	**$^1S_2SOSO$**	**-12.4**	-12.2	-13.5
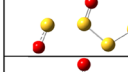	$^1S_2SOSO \rightarrow$ **^{1}TS2-1** $\rightarrow$ $^1S_3O + {}^3SO$	26.6	**25.1**	25.4
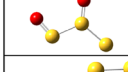	$^1S_2SOSO \rightarrow$ **^{1}TS2-2** $\rightarrow$ $^1SSOSO + {}^3S$ See continuation of SSOSO in Table 1 and Fig.9	51.2	**40.0**	51.9
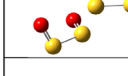	$^1S_2SOSO \rightarrow$ **^{1}TS2-3** $\rightarrow$ $^3S_2$ + cis-^{1}OSSO	-	**2.6**	-
Channel-3				
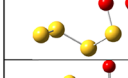	$^3S_4O_2 \rightarrow$ **^{1}TS3** $\rightarrow$ $^3S_3SO_2$	76.5	79.3	**76.6**
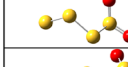	**$^3S_3SO_2$**	-7.9	-6.1	**-8.4**
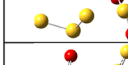	$^3S_3SO_2 \rightarrow$ **^{3}TS3-1** $\rightarrow$ $^1S_3 + {}^1SO_2$	**-10.2**	-3.4	-9.1
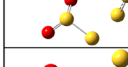	$^3S_3SO_2 \rightarrow$ **^{3}TS3-2** $\rightarrow$ $^3S_2 + {}^1SSO_2$	-	**-4.7**	-4.0
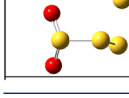	$S_3SO_2 \rightarrow$ **^{3}TS3-3**$\rightarrow$ $^3S + {}^3S_2SO_2$ See Table 1 and Fig. 9 for continuation	15.6	**16.2**	17.3

(*continued*).

Table 3. Continued.

Channel-4				
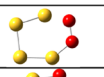	$^3S_4O_2 \rightarrow$ **^{3}TS4** $\rightarrow {}^3Y(S_4O_2)$	**78.7**	TST not found	TST not found
	**$^3Y(S_4O_2)$**	75.0	**76.7**	75.5
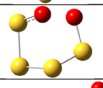	$^3Y(S_4O_2) \rightarrow$ **^{1}TS4-1** $\rightarrow {}^3OS_4O$	39.9	36.9	**37.9**
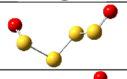	**$^3OS_4O$**	-16.9	-17.8	**-16.5**
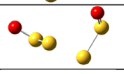	$^3OS_4O \rightarrow$ **^{3}TS4-2** $\rightarrow 2\ {}^1S_2O$	-	**-12.1**	-
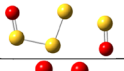	$^3OS_4O \rightarrow$ **^{3}TS4-3** $\rightarrow {}^1S_3O + {}^3SO$	-	**-1.5**	-
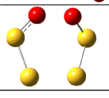	$^3Y(S4O2) \rightarrow$ **^{3}TS4-4** $\rightarrow 2\ {}^1S_2O$	**41.5**	-	42.5
Channel-5				
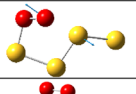	$S_4O_2 \rightarrow$ **^{3}TS5** $\rightarrow {}^1SY(S_3O_2)$	**92.9**	106.4	95.0
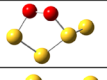	**$^1SY(S_3O_2)$**	48.0	47.4	**46.9**
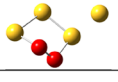	$^1SY(S_3O_2) \rightarrow$ **^{1}TS5-1** $\rightarrow {}^3S + {}^1Y(S_3O_2)$ See continuation of $Y(S_3O_2)$ in Table 1 and Fig. 9	88.6	**88.4**	89.6
Channel-6				
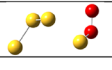	$S_4O_2 \rightarrow$ **^{1}TS6** $\rightarrow {}^1S_3 + {}^1SOO$	71.4	70.4	**69.1**
Channel-7				
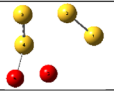	$S_4O_2 \rightarrow$ **^{1}TS7** $\rightarrow {}^3S_2 + {}^1SSO_2$	79.7	**85.3**	
Channel-8				
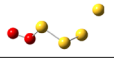	$S_4O_2 \rightarrow$ **^{3}TS8** $\rightarrow {}^3S + {}^1S_3O_2$	76.0	**76.8**	76.9

3.1.1.2. Attack of O_2 at the central sulfur atom of S_3. The reactions initiated by the attack of $^3O_2$ at the central sulfur atom of $^3S_3$ are illustrated in Table 2 together with the calculated enthalpies of formation for the resulting species and transition state structures. Addition of $^3O_2$ to the central sulfur atom proceeds via transition state **TSB-a**, leading to formation of a different peroxy radical iso-S_3O_2.

Among the applied computational methods, the G3 calculation yields the highest enthalpy for this step; however, this value is selected because it provides the most reliable transition-state geometry. Examination of the vibrational frequencies and their corresponding displacement vectors clearly shows the oxygen and central sulfur atoms moving toward each other to form the iso-S_3O_2 intermediate. This characteristic motion is not observed with the other computational methods.

The resulting iso-S_3O_2 intermediates subsequently reacts through four different pathways, as listed in Table 2. For these subsequent steps, the calculated energies show good agreement across the three applied methods

In addition, the calculations indicate that the addition of O_2 to $^1S_3$ can proceed via an alternative pathway (**TSB-b**), in which an S–S bond is cleaved, leading to the formation of S_2O_2.

The TSB-b transition-state structures obtained at the G3 and G4 levels clearly show the simultaneous approach of O_2 toward sulfur and the cleavage of an S–S bond resulting in S_2O_2 formation. In contrast, this characteristic motion is not observed at the CBS-QB3 level, which explains the difference in the calculated enthalpy at that level of theory. The subsequent reactions of S_2O_2 have been described in Ref. [16].

3.1.2. $S_4 + {}^3O_2$ system

3.1.2.1. Attack of O_2 at terminal sulfur atom of S_4. Similar to the $^1S_3 + {}^3O_2$ system, two sulfur sites are available for oxygen addition in the $^1S_4 + {}^3O_2$ system reaction: the terminal and the inner sulfur atom (see Figure 1). Addition of $^3O_2$ at the terminal sulfur atom of $^1S_4$ forms a peroxy radical S_4O_2 which, analogous to $^1S_3O_2$, undergoes subsequent reactions (bond scissions and rearrangements) through eight distinct reaction pathways.

Table 3 summarizes the standard enthalpies of formation for all species and transition state structures involved in the reactions resulting from addition of $^3O_2$ at the terminal sulfur atom. The structures of the identified transition states and their corresponding reaction pathways from reactants to intermediates/products are also presented in Table 3. For most intermediates and transition states, only small deviations in enthalpy are observed among the three applied computational methods, indicating overall good agreement.

Exceptions are **TS2**, **TS2-2**, **TS3-1**, **TS5**, and **TS7**, where one of the methods deviates by approximately 10.0 kcal mol^{-1}. To determine the most reliable values, the vibrational frequencies were carefully examined. For **TS2-2**, the calculated activation energies are 40.0 kcal mol^{-1} (G3) and 51.2 kcal mol^{-1} (CBS-QB3). As illustrated in Figure 5, the optimized geometries obtained by the two methods are quite similar. However, the displacement vectors associated with the imaginary frequency differ: in the G3 calculation (Figure 5, left), the motion corresponds to S–S bond dissociation, whereas in the CBS-QB3 result (Figure 5, right), the displacement resembles sulfur addition. This difference in the transition mode may explain the discrepancy in the calculated energy barriers. The enthalpy calculated at the G4 level is not shown in Figure 5 because the optimized structure and dihedral angles as well as the calculated energies are identical to those obtained at the CBS-QB3 level.

The displacement vectors for **TS2** and **TS5** were also examined and used to guide the selection of the most reliable calculated energy values. For TS7, the G3-calculated energy is preferred because the corresponding imaginary frequency shows both the S-S bond cleavage and migration of the oxygen atom to S-4 to form SSO_2. In contrast, the CBS-QB3 structure does not capture this combined motion, see Figure 6. The G4 enthalpy is not shown in Figure 6 as its structure, dihedral angles, and energy are identical to CBS-QB3.

3.1.2.2. Attack of O_2 at the inner sulfur atom of S_4. Table 4 summarizes the species and transition-state structures involved in the reactions initiated by the attack of $^3O_2$at the inner sulfur atom of $^1S_4$.

Table 4. Attack of O_2 at the inner sulfur atom of S_4. Standard enthalpy of formation ($\Delta_f H^0_{298}$) and transition state structures (ΔH_{TS})resulting from species involved in the $^1S_4 + {}^3O_2$ system calculated at CBS-QB3, G3 and G4 levels in kcal mol^{-1}, Y means cyclic.

Structure	Reactions for $\Delta_f H^0_{298}$ and ΔH_{TS} calculation	$\Delta_f H^0_{298}$ in kcal mol^{-1}		
		CBS-QB3	G3	G4
Reference data: ^3S: 66.24; $^3S_2$: 30.74; ^3SO: 1.2; $^1SO_2$: -70.94; ^1S_2O: -13.5; ^3O: 58; ^1SOO: 45.8				
Addition of O_2 on the inner sulfur atom of S_4				
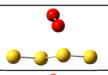	$^1S_4 + O_2 \rightarrow$ **^{3}TSB-a** $\rightarrow {}^3$iso-S_4O_2	67.3	**74.72**	68.4
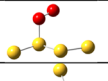	**^{3}iso-S_4O_2**	**69.3**	71.2	70.4
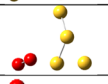	$^1S_4 + O_2 \rightarrow$ **^{3}TSB-b** $\rightarrow {}^3S + {}^1S_3O_2$	98.8	113.8	**102.0**
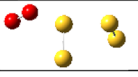	$^1S_4 + O_2 \rightarrow$ **^{3}TSB-c** $\rightarrow {}^3S_2 + {}^1S_2O_2$	81.4	88.7	**85.7**
Channel-1				
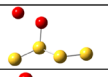	$S_3O_2S \rightarrow$ **^{3}TS1** $\rightarrow$ iso-$^3S_4O + {}^3O$	98.5	112.4	**101.2**
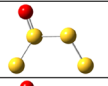	**^{3}iso-S_4O**	**38.3**	38.8	38.2
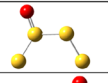	**^{1}iso-S_4O**	**30.4**	30.8	31.2
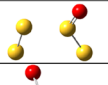	iso-$S_4O \rightarrow$ **^{1}TS1-1** $\rightarrow {}^1S_2O + {}^3S_2$	33.7	**32.8**	33.4
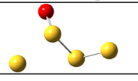	iso-$S_4O \rightarrow$ **^{3}TS1-2** $\rightarrow {}^1S_3O + {}^3S$	51.2	**51.6**	50.8
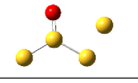	iso-$S_4O \rightarrow$ **^{1}TS1-3** $\rightarrow$ iso-$^1S_3O + {}^3S$	73.2	**74.3**	73.9
Channel-2				
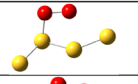	^{3}iso-$S_4O_2 \rightarrow$ **^{3}TS2** $\rightarrow {}^1$SY(S_2O_2)S	125.5	129.5	**125.1**
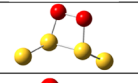	**^{1}SY(S_2O_2)S**	74.3	74.1	**74.1**
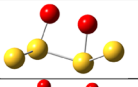	^{1}SY(S_2O_2)S $\rightarrow$ **^{1}TS2-1** $\rightarrow {}^1$cis-S(SOSO)S	95.0	**87.7**	101.6
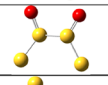	**^{1}cis-S(SOSO)S**	**11.8**	14.4	12.5
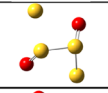	^{1}cis-S(SOSO)S $\rightarrow$ **^{3}TS2-2** $\rightarrow {}^3S + {}^3$SSOSO	37.0	**39.2**	37.5
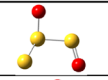	**^{3}SSOSO**	19.1	19.4	**18.6**
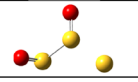	^{3}SSOSO $\rightarrow$ **^{3}TS2-3** $\rightarrow {}^3S + {}^1$cis-OSSO cis-OSSO: -30.44 at G3 level [Ref. 16]	20.7	**20.6**	20.9
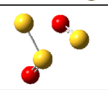	^{3}SSOSO $\rightarrow$ **^{3}TS2-4** $\rightarrow {}^1S_2O + {}^3$SO	TST not found	**17.4**	TST not found

(*continued*).

Table 4. Continued.

Channel-3				
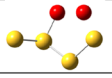	^{3}iso-S_4O_2 → **^{3}TS3** → $^{1}SY(S_3O_2)$ Continuation of $^{1}SY(S_3O_2)$ in Table 3 and Fig. 13	98.9	**99.8**	99.4
Channel-4				
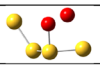	^{3}iso-S_4O_2 → **^{3}TS4** → S_2SOSO Continuation of S_2SOSO in Table 3 and Fig. 13	106.9	**106.3**	107.2
Channel-5				
	^{3}iso-S_4O_2 → **^{1}TS5** → $^{1}S_2SO_2S$	91.1	**90.7**	79.1
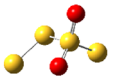	**$^{3}S_2(SO_2)S$**	4.73	**7.38**	2.41
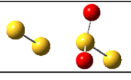	$S_2(SO_2)S$ → **^{3}TS5-1** → $^{3}S_2 + {}^{1}SSO_2$	2.80	**1.87**	TST not found
Channel-6				
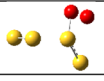	^{3}iso-S_4O_2 → **^{1}TS6** → $^{3}S_2 + {}^{1}SSO_2$	91.3	**93.6**	90.7
Channel-7				
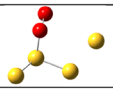	^{3}iso-S_4O_2 → **^{3}TS7** → ^{3}S + iso-$^{3}S_3O_2$	92.5	**100.8**	93.8
Channel-8				
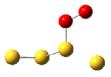	^{3}iso-S_4O_2 → **^{3}TS8** → $^{3}S + {}^{1}S_3O_2$	**100.5**	104.0	103.6

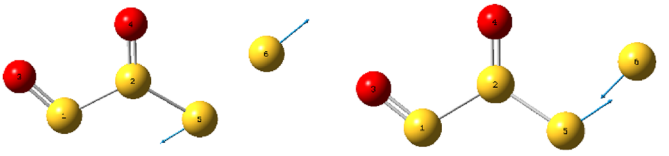

Figure 5. Illustration of the transition state structure **TS2-2** from G3 calculation (left) and CBS-QB3 calculation (right).

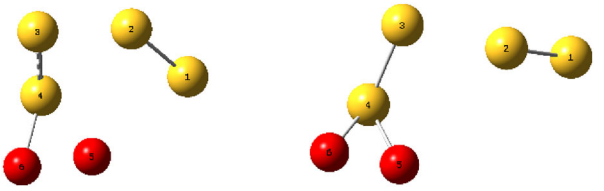

Figure 6. Illustration of the transition state structure **TS7** from G3 calculations (left) and CBS-QB3 calculations (right).

Analogous to the $^{1}S_3 + O_2$ system, addition of $^{3}O_2$ to the inner sulfur of S_4 proceeds via two reactions: Direct addition forming an iso-peroxy radical, ^{3}iso-S_4O_2 via (**TSB-a**) and S–S bond cleavage via (**TSB-b**), leading to formation of $^{1}S_3O_2$. The subsequent reactions

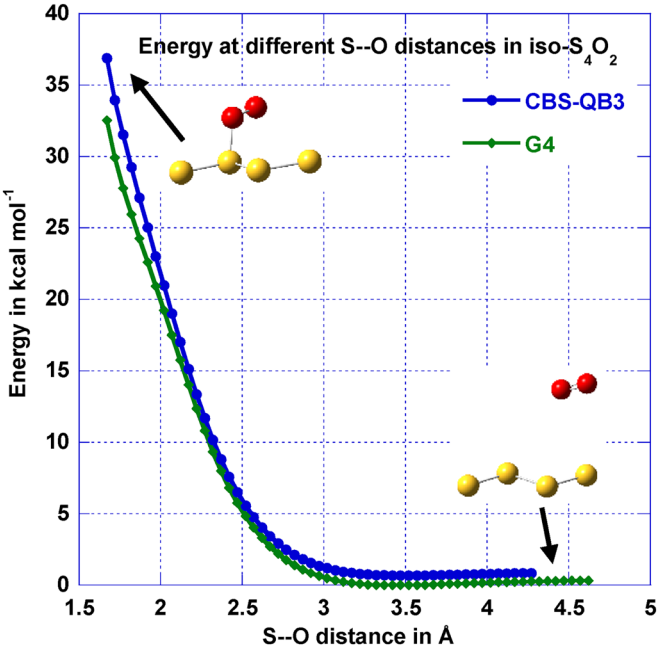

Figure 7. Potential Energy curve of the S-OO bond scission in iso-S_4O_2.

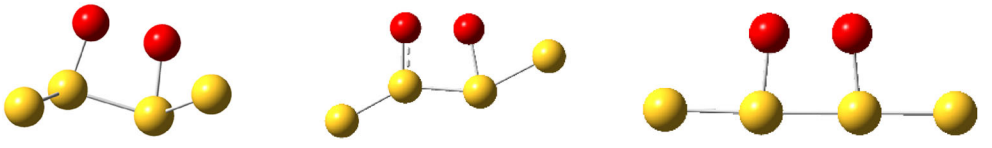

Figure 8. Illustration of the transition state structure **TS2-1** from G3 calculation (left) and CBS-QB3 calculation (middle) and G4 (right).

of $^1S_3O_2$ are described in Table 1, whereas the bond scission and rearrangement reactions of ^{3}iso-S_4O_2 are presented in Table 4.

In addition, a third reaction pathway is identified for this system: An alternative S–S bond cleavage (**TSB-c**) occurs, resulting in the formation of S_2 and S_2O_2. The further degradation reactions of S_2O_2 are described in Ref. [16].

For the subsequent reactions of ^{3}iso-S_4O_2, seven possible pathways have been identified (see Table 4). As described above, the recommended enthalpy values were selected after examination of the optimized geometries and the associated vibrational frequencies of the intermediates and transition states. Consequently, the transition state with the lowest calculated energy was not automatically chosen in every case; instead, the structure that most consistently represents the intended reaction was preferred. For nearly all species, a reasonable agreement among the applied computational methods is observed.

Notable exceptions are **TSB-b** and **TS2-1**, which exhibit significant deviations in their calculated energies. For **TSB-b**, the G3 result is selected because the corresponding imaginary frequency clearly indicates the simultaneous approach of oxygen and S-S bond cleavage, consistent with the expected reaction.

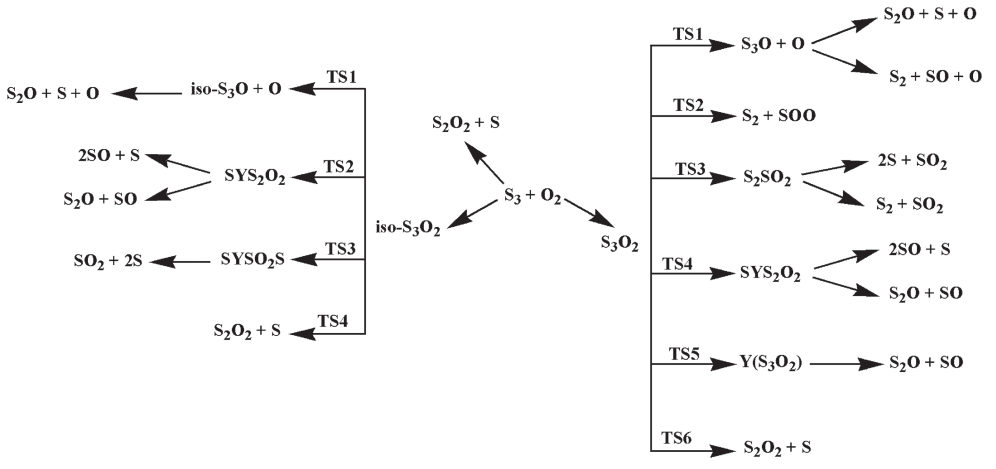

Figure 9. Reaction channels resulting from the attack of O_2 at the terminal (right) and central (left) sulfur of $^1S_3$.

Surprisingly, no saddle point corresponding to **TSB-a** could be located. To validate the enthalpy for this transition state, a potential energy scan was performed at different S–OO bond distance in S_4O_2, effectively probing the dissociation energy for the reaction $S_4O_2 \rightarrow S_4 + O_2$.

The S–OO distance was incrementally increased by 0.05 Å, ranging from 1.67 Å up to approximately 4 Å, and each structure was optimized at both G4 and CBS-QB3 levels. The resulting potential energy surface, shown in Figure 7, confirms a barrierless association of O_2. Both the G4 and CBS-QB3 curves are smooth and continuous, and they yield very similar energy profiles, with similar barriers of 32.5 kcal mol^{-1} (G4) and 36.9 kcal mol^{-1} (CBS-QB3). These values are consistent with the G3-calculated energy barrier of 32.2 kcal mol^{-1} relative to $S_4 + O_2$, supporting the reliability of the barrierless calculated **TSB-a**.

The second transition state exhibiting significant deviations among the computational methods is **TS2-1**. These differences in the calculated energies can be attributed to variations in the optimized geometries. As shown in Figure 8, the SS-SS dihedral angles differ markedly across the methods: –51.84° for G3, 179.96° for CBS-QB3, and 69.22° for G4. Such large discrepancies in the dihedral angles significantly affect the electronic interactions and steric strain in the transition state, leading to the observed variations in the calculated energy barriers.

3.2. Reactions and potential energy diagrams

3.2.1. The $^1S_3 + {}^3O_2$ reaction system

Figure 9 depicts possible reaction channels for the attack of $^3O_2$ at the terminal sulfur of $^1S_3$ (right part of the figure) and for the attack at the central sulfur atom (left part of the figure). The same products, viz. S_2O, SO, S, S_2, and SO_2, evolve from the reactions. The single channels are discussed in the following sections.

3.2.1.1. Attack of O_2 at the terminal sulfur atom of S_3. Figure 10 depicts the reaction channels for the attack of O_2 at the terminal sulfur of S_3. The peroxy intermediate S_3O_2 is formed over a barrier of 26.8 kcal mol^{-1} relative to $S_3 + O_2$ at 33.8 kcal mol^{-1}. S_3O_2 can subsequently react through six distinct pathways.

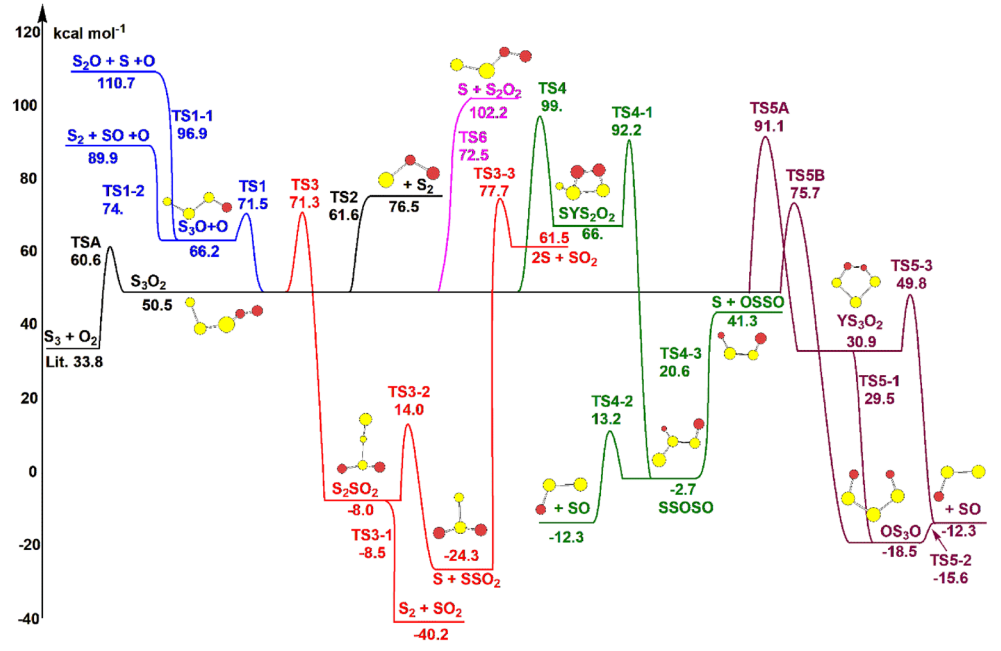

Figure 10. Potential diagram for the attack of $^3O_2$ on the terminal sulfur atom of $^1S_3$. Values represent the recommended enthalpies in kcal mol^{-1} as listed in Table 1. Electron spin multiplicity as given in Table 1.

The first subsequent pathway of S_3O_2 involves O-O (**TS1**) bond scission with a barrier of 21 kcal mol^{-1} forming S_3O which then undergoes S-S bond scission via two different reactions. Formation of $S_2O + S$ through **TS1-1**, with a barrier of 30.7 kcal mol^{-1} relative to S_3O and formation of $S_2 + SO$ via **TS1-2**, with a lower barrier of 7.7 kcal mol^{-1} relative to S_3O.

The second pathway (**TS2**) corresponds to the simple dissociation S_3O_2 into $S_2 + SOO$, which occurs over a relatively low barrier of 11.1 kcal mol^{-1}.

The third pathway is controlled by the ipso addition of the oxygen via **TS3**. Due of the high strain in the three-membered ring, the initially formed species S_2YSO_2 (not shown in Figure 10) is highly unstable and rapidly undergoes ring opening to yield the more stable S_2SO_2, which lies at -8.0 kcal mol^{-1} relative to the reactants (see Figure 10). The energy barrier for this reaction is 20.8 kcal mol^{-1} relative to S_3O_2. In S_2SO_2, cleavage of the two S–S bonds can proceed via two distinct pathways: a barrierless dissociation to $S_2 + SO_2$ (**TS3-1**), or via a transition state (**TS3-2**) with an activation barrier of 21.4 kcal mol^{-1} leading to $S + SSO_2$. The SSO_2 fragment formed in the latter pathway is relatively low at -41.9 kcal mol^{-1} can further dissociate to $2S + SO_2$ over a high barrier of ca. 54 kcal mol^{-1} (**TS3-3**).

The fourth reaction pathway proceeds through the formation of a cyclic four-membered ring $SY(S_2O_2)$ in which each oxygen atom is bonded to a different sulfur atom. This occurs over a barrier of 48.5 kcal mol^{-1} (**TS4**) relative to S_3O_2. The resulting isomer, lying at 66 kcal mol^{-1} $SY(S_2O_2)$ contains a highly strained Y(SSOO) cycle and can easily undergo ring opening (**TS4-1**) over 26.2 kcal mol^{-1} yielding to a lower-energy compound SSOSO at -2.7 kcal mol^{1}. SSOSO dissociates further at different levels of energy to SSO + SO (**TS4-2**) and to S + cis-OSSO (**TS4-3**) via 15.9 kcal mol^{-1} and 23.3 kcal mol^{-1}, respectively.

The G3 method identified the formation of the cyclic $Y(S_3O_2)$ isomer formed via about 40.6 kcal mol^{-1} (**TS5A**) relative to the peroxy intermediate S_3O_2 (50.5 kcal mol^{-1}). Two successive reactions identified for this $Y(S_3O_2)$ isomer at 30.9 kcal mol^{-1}, in which both oxygen atoms are part of the ring, are observed: A barrierless ring opening (**TS5-1**) leading to the opened ^{3}OS3O isomer at -18.1 kcal mol^{-1} followed by a S–S bond cleavage (**TS5-2**) requiring only 2.9 kcal mol^{-1} to form $S_2O + SO$. Additionally, the G3 calculations identify an alternative dissociation of $Y(S_3O_2)$ via some 18.9 kcal mol^{-1} (**TS5-3**) relative to $Y(S_3O_2)$ resulting also in the formation of $S_2O + SO$. In contrast, CBS-QB3 and G4 calculations predict a different transition state structure, **TS5B**, corresponding to a direct conversion of S_3O_2 to OS_3O via a lower barrier at 25.2 kcal mol^{-1}.

The last possible reaction pathway of the S_3O_2 peroxy involves elimination of a sulfur atom (**TS6**) by overcoming some 22 kcal mol^{-1} relative to S_3O_2.

3.2.1.2. Attack of O_2 at the central sulfur atom of S_3. The attack of O_2 at the ventral atom of S_3 results in the formation of the iso-S_3O_2 isomer over a barrier of 60.6 kcal mol^{-1} (**TSB-a**) relative to $S_3 + O_2$ (see Figure 11). A second pathway involves S–S bond scission (**TSB-b**), forming S_2O_2, which has been previously investigated [16]. This reaction proceeds over a slightly higher barrier of 67.5 kcal mol^{-1} relative to the entrance channel $S_3 + O_2$. Four channels are opened for subsequent reactions of the iso-S_3O_2 isomer. Channel-1 involves O–O bond scission of iso-S_3O_2 to form iso-S_3O + O. This bond scission (**TS1**) requires 27.1 kcal mol^{-1} relative to the peroxy iso-S_3O_2. The resulting iso-S_3O intermediate can then undergo S – S bond cleavage (**TS1-1**) via a barrier of 32.9 kcal mol^{-1}, leading to the formation of the products $S_2O + S$.

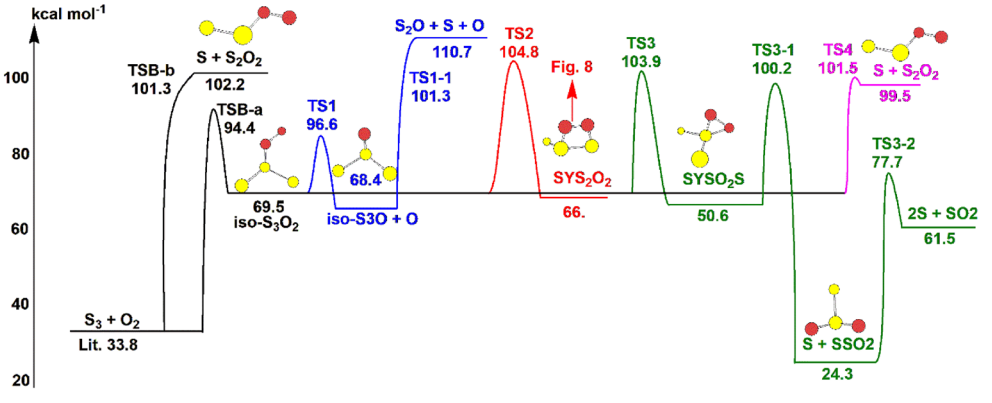

Figure 11. Potential diagram for the attack of O_2 at the central sulfur atom of $^1S_3$. Values represent the recommended enthalpies in kcal mol^{-1} as listed in Table 2. Electron spin multiplicity as given in Table 2.

Channel 2 involves attack of the terminal oxygen on the adjacent sulfur atom via **TS2**, with a barrier of 35.3 kcal mol^{-1} (see Figure 11). This reaction forms the same strained four-membered ring intermediate, SYS_2O_2, as observed in channel 4 of the oxygen attack at the terminal sulfur. The subsequent reactions of this intermediate are described in Table 1 and in the previous section.

Channel 3 proceeds through ipso-addition of the oxygen via **TS3**. The resulting $SYSO_2S$ species, illustrated in Figure 11, contains a three-membered ring and is formed at 50.6 kcal mol^{-1}, with a reaction barrier of 34.4 kcal mol^{-1} above iso-S_3O_2. This The $SYSO_2S$ intermediate undergoes simultaneous cleavage of the weak peroxy O–O bond and elimination of one sulfur atom over 49.6 kcal mol^{-1} (**TS3-1**), yielding the stable, low-energy products $SSO_2 + S$. The further dissociation of SSO_2 (**TS3-2**) is described in Figure 10 and corresponds to TS3-3.

Channel 4 corresponds to the simple elimination of one sulfur atom (**TS4**), which occurs over 32.0 kcal mol^{-1} relative to $S_3 + O_2$ and producing $S + S_2O_2$ (investigated in Ref. [16]).

3.2.2. The $^1S_4 + {}^3O_2$ reaction system

Figure 12 depicts the major channels for the attack of O_2 at the terminal sulfur of S_4 (right) and at the inner sulfur atom (left). The final products are similar to those of the $^1S_3 + {}^3O_2$ reaction system, S_2O, SO, S, S_2, and SO_2. Detailed discussion of the channels is given in the following sections.

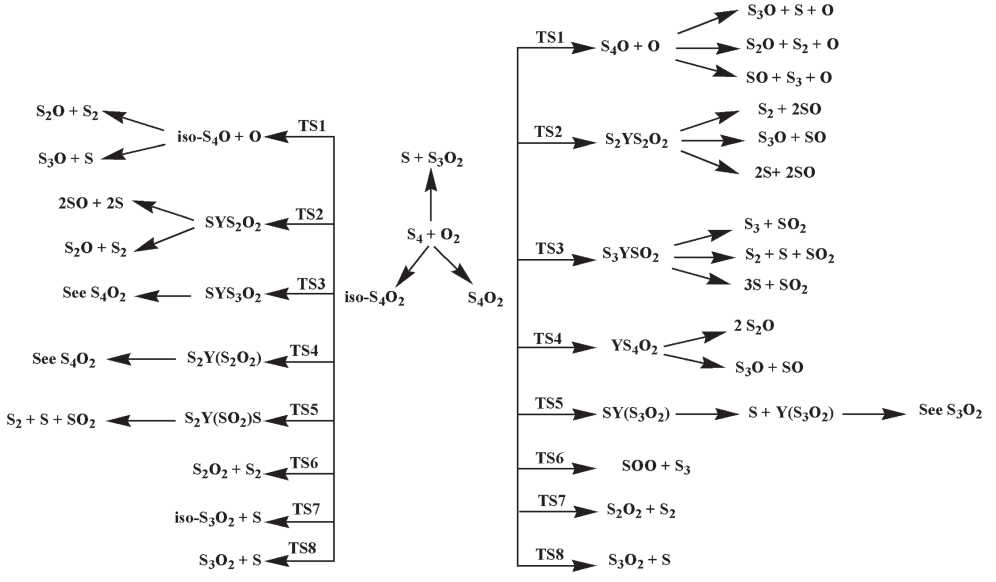

Figure 12. Reaction channels resulting from the attack of O_2 at the terminal (right) and inner (left) sulfur of $^1S_4$.

3.2.2.1. Attack of O_2 at the terminal sulfur atom of S_4. Figure 13 illustrates the possible reaction channels following O_2 attack at the terminal sulfur of S_4. The peroxy intermediate S_4O_2 is formed over a barrier of 36.1 kcal mol^{-1} relative to $S_4 + O_2$ at 34.9 kcal mol^{-1}. Notably, O_2 addition to S_4 requires about 10.0 kcal mol^{-1} more energy than to S_3, see above section.

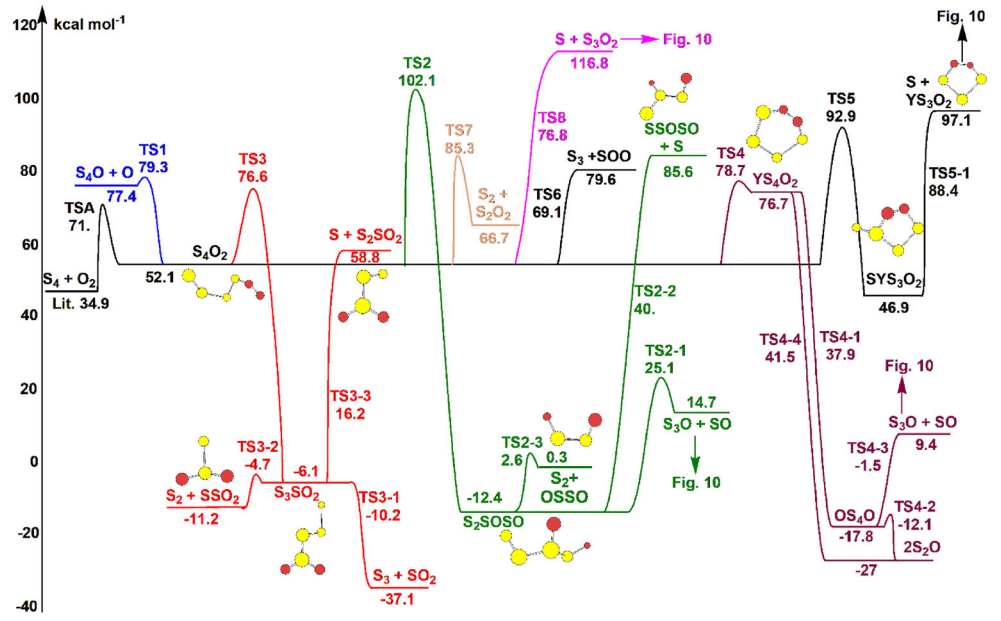

Figure 13. Potential diagram for the attack of O_2 at the terminal sulfur atom of $^1S_4$. Values represent the recommended enthalpies in kcal mol^{-1} as listed in Table 3. Electron spin multiplicity as given in Table 3.

The S_4O_2 peroxy intermediate can undergo subsequent reactions/bond scissions via eight pathways. Similar to S_3O_2 peroxy, S_4O_2 undergoes a O-O (**TS1**) bond scission over a 27.2 kcal mol^{-1} energy barrier relative to S_4O_2. We note that the O–O bond cleavage energy is comparable to that of S_3O_2 differing by less than 3 kcal mol^{-1}. This cleavage produces $S_4O + O$. S_4O can then undergo three subsequent S–S bond scissions conducting to $S + S_3O$ (**TS1-1**) over 24.3 kcal mol^{-1}, to $S_2 + S_2O$ (**TS1-2**) without barrier, and to $S_3 + SO$ (**TS1-3**) over 23 kcal mol^{-1}, all relative to S_4O (see Table 3). As observed for S_3O degradation, the energy required to eliminate a single sulfur atom is similar in both systems, approximately 22–24 kcal mol^{-1}.

Channel-2 is proceeds via addition of oxygen to the adjacent sulfur atom (**TS2**) over a 50 kcal mol^{-1} relative to S_4O_2. As calculated for S_3O_2, addition of oxygen to a central sulfur requires more energy. The resulting isomer $S_2Y(S_2O_2)$ (not illustrated in Figure 13) is highly unstable because of its strained ring structure and high internal energy. Consequently, it undergoes an immediate, barrierless ring-opening reaction to yield the more stable species S_2SOSO, which is 12.4 kcal mol^{-1} lower in energy. This species can then dissociate into products at different levels of energy: $S_3O + SO$ (**TS2-1**), $S + SSOSO$ (**TS2-2**) and $S_2 + $ cis-OSSO (**TS2-3**) via 37.5 kcal mol^{-1}, 52.4 kcal mol^{-1} and 15.0 kcal mol^{-1}, respectively.

Figure 13 also depicts the third pathway, involving ipso addition of the oxygen via **TS3** over a 24.5 kcal mol^{-1}. This barrier is comparable to the ipso addition in S_3O_2, calculated at 20.8 kcal mol^{-1}.

The resulting species, S_3YSO_2 (not shown in Figure 13), contains a highly strained three-membered ring. This ring undergoes a barrierless opening to yield the more stable species S_3SO_2, which lies 6.1 kcal mol^{-1} lower in energy. S_3SO_2 then degrades via three transition

state structures to $S_3 + SO_2$ (**TS3-1**) with no barrier, $S_2 + SSO_2$ (**TS3-2**) over 1.4 kcal mol^{-1} and $S + S_2SO_2$ (**TS3-3**) over 22.3 kcal mol^{-1}. Subsequent reactions of the S_2SO_2 isomer are illustrated in Table 1 and Figure 10.

The fourth pathway proceeds via formation of a cyclic six-membered ring $Y(S_4O_2)$ at 76.7 kcal mol^{-1}, in which both oxygens are incorporated into the ring. This cyclic isomer forms by overcoming a barrier of 26.6 kcal mol^{-1} (**TS4**) relative to the peroxy S_4O_2 intermediate at 52.1 kcal mol^{-1}. The energy required for ring closure of $Y(S_4O_2)$ is comparable to that calculated for $Y(S_3O_2)$. As observed for the latter, the weak O-O bond in $Y(S_4O_2)$ cleaves without barrier (**TS4-1**), forming OS_4O at -17.8 kcal mol^{-1}. Subsequent S-S bond scissions of OS_4O, identified only at the G3 level, occurs with a relatively low barrier of 5.7 kcal mol^{-1} (**TS4-2**). Cleavage of the OSS–SSO bond (**TS4-2**) forms $2S_2O$ whereas scission of the OSSS–SO results in $S_3O + SO$ (**TS4-3**). Additionally, a direct barrierless bond cleavage of $Y(S_4O_2)$ (**TS4-4**) conducts to formation of $2S_2O$.

The fifth possible reaction pathway for the S_4O_2 peroxy involves the attack of the oxygen on the inner sulfur atom, as illustrated in Figure 13 and Table 3. This addition (**TS5**) requires 40.8 kcal mol^{-1} relative to S_4O_2 and lead to formation of a new isomer $SY(S_3O_2)$ at 46.9 kcal mol^{-1}.

The energy barrier necessary for the formation of a five-membered ring (YS_3O_2) is similar to that required for the closure of S_3O_2 at 40.6 kcal mol^{-1}. $SY(S_3O_2)$ subsequently undergoes a S – S bond cleavage (**TS5-1**) over a barrier of 41.5 kcal·mol^{-1}, yielding $S + Y(S_3O_2)$. The further dissociation pathways of $Y(S_3O_2)$ are discussed in section 2.1.

Channel-6 (**TS6**) consists of the simple bond cleavage of S_4O_2 to $S_3 + SOO$ over a relatively low barrier of 17 kcal mol^{-1}. This value is comparable to the analogous reaction of S_3O_2 to $S_2 + SOO$ at 11 kcal mol^{-1}.

In channel 7 (**TS7**), S_4O_2 undergoes a simple bond scission, requiring an energy barrier of 33.2 kcal mol^{-1} to form S $S_2 + S_2O_2$.

In the final pathway, channel-8 (**TS8**), elimination of one sulfur atom occurs over 24.7 kcal mol^{-1} barrier relative to S_4O_2 producing $S + S_3O_2$. This barrier is similar to that of the corresponding reaction in S_3O_2, which forms $S + S_2O_2$ with 21.9 kcal mol^{-1} energy barrier.

3.2.2.2. Attack of O_2 at the inner sulfur atom of S_4. Similar to the $S_3 + O_2$ system, oxygen can also attack an inner sulfur atom of S_4, leading to the formation of an iso-S_4O_2 isomer (see Figure 14 and Table 4). The barrier for this reaction (**TSB-a**) is 32.2 kcal mol^{-1} relative to $S_4 + O_2$. This result indicates that O_2 addition to S_4 is significantly more favorable than to S_3. A second possible mode of attack of O_2 results in sulfur atom elimination and formation of S_3O_2 which is discussed in section 2.1. This reaction proceeds via 67.2 kcal mol^{-1} (**TSB-b**) relative to $S_4 + O_2$, which is comparable to the analogous $S_3 + O_2$ reaction at 67.9 kcal mol^{-1}. A third reaction resulting from the oxygen attack is governed by the second S – S bond cleavage and resulting in $S_2 + S_2O_2$ (**TSB-c**). This process requires a lower barrier of 50.8 kcal mol^{-1} relative to $S_4 + O_2$.

Eight consecutive reaction channels are possible for the iso-S_4O_2 isomer. Cleavage of the O-O bond in the peroxy iso-S_4O_2 to form iso-$S_4O + O$ (**TS1**) exhibits a barrier of 31.9 kcal mol^{-1} relative to the S_4O_2 peroxy. This value is similar to that calculated for S_3O_2, which undergoes O-O bond scission over 27.1 kcal mol^{-1}.

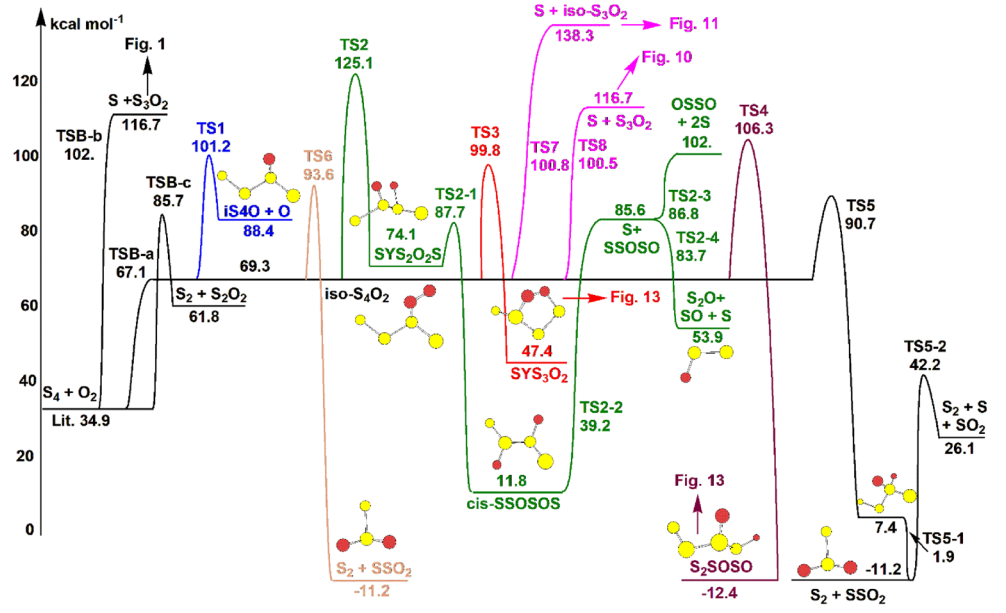

Figure 14. Potential diagram for the attack of O_2 at the inner sulfur atom of $^1S_4$. Values represent the recommended enthalpies in kcal mol^{-1} as listed in Table 4. Electron spin multiplicity as given in Table 4.

For iso-S_4O, both singlet and triplet compounds could be calculated at 30.4 kcal mol^{-1} and 38.3 kcal mol^{-1}, respectively. Subsequent S-S bond cleavage of iso-S_4O can occur along three possible pathways: formation of $S_2O + S_2$ (**TS1-1**) via a low energy barrier of 2.4 kcal mol^{-1}, formation of $S_3O + S$ (**TS1-2**) via 21.2 kcal mol^{-1} and formation of iso-$S_3O + S$ (**TS1-3**) via a higher barrier of 43.9 kcal mol^{-1}, all relative to singlet iso-S_4O (see Table 4).

Attack of the terminal oxygen at the adjacent centered sulfur atom (**TS2**), illustrated in Figure 14 and Table 4, leads to formation of the isomer SYS_2O_2S calculated at 74.1 kcal mol^{-1}. This species contains a four-membered ring (YSOOS) located at the center of the structure. The barrier required for its formation is 55.8 kcal mol^{-1} relative to iso-S_4O_2.

SYS_2O_2S subsequently undergoes ring opening (**TS2-1**) through a relatively low barrier of 13.6 kcal mol^{-1} forming a new isomer, cis-S(SOSO)S, at 11.8 kcal mol^{-1}. Successive dissociation of cis-S(SOSO)S consists of sulfur atom elimination (**TS2-2**) over 27.4 kcal mol^{-1} to form SSOSO. This intermediate reacts further through two transition state structures resulting in formation of S + OSSO (**TS2-3**) over only 2 kcal mol^{-1} and barrierless formation of S_2O + SO (**TS2-4**).

The third pathway (**TS3**) includes the formation of a five-membered ring intermediate, $SY(S_3O_2)$, within iso-S_4O_2, proceeding over 30.5 kcal mol^{-1} energy barrier. The subsequent reactions of $SY(S_3O_2)$ have been discussed in section 2.1.

Channel-4 involves an oxygen attack at the adjacent terminal sulfur atom (TS4), proceeding over an energy barrier of 37.0 kcal mol^{-1} relative to S_4O_2, and resulting in the formation of $S_2Y(S_2O_2)$. This pathway closely parallels the oxygen addition mechanism observed in the iso-S_3O_2 system, where $SY(S_2O_2)$ is formed through a similar barrier of 35.3 kcal mol^{-1}.

The intermediate $S_2Y(S_2O_2)$ produced in this channel is identical to that generated via Channel-2 of the subsequent S_4O_2 reaction. As discussed previously, this isomer is unstable and undergoes an immediate, barrierless ring-opening process to form S_2SOSO, which lies at 12.4 kcal mol^{-1}. The subsequent transformations of this intermediate have been described above.

The fifth reaction pathway (**TS5**) involves an alternative oxygen addition at the ipso position, forming the highly unstable intermediate $S_2Y(SO_2)S$ (not represented in Figure 14). Owing to the pronounced three-membered ring strain, this species undergoes cleavage of the weak O-O bond to form the significantly more stable isomer S_2SO_2S, which lies lower in energy at 7.4 kcal mol^{-1}. Subsequently, fragmentation occurs via cleavage of the adjacent S-S bond (**TS5-1**), ultimately yielding S_2 and SSO_2. Although SSO_2 is thermodynamically stable (-41.9 kcal mol^{-1}), it may, under suitable conditions dissociate through S – S bond cleavage over a 53.4 kcal mol^{-1} barrier (**TS5-2**), yielding $S + SO_2$.

The iso-S_4O_2 peroxy may also undergo direct S-S bond scission (**TS6**) forming SSO_2 through 24.3 kcal mol^{-1} energy barrier. The final two pathways identified for iso-S_4O_2 correspond to simple terminal sulfur eliminations from either end of iso-S_4O_2 as illustrated in Table 4.

In the first case (**TS7**), sulfur atom loss produces $S +$ iso-S_3O_2 and in the second one (**TS8**) leads to $S + S_3O_2$ over 31.5 and 31.2 kcal mol^{-1}, respectively. These dissociation channels closely parallel the behavior observed for iso-S_3O_2, for which fragmentation to $S + S_2O_2$ was calculated to occur at 32.0 kcal mol^{-1}. In all cases, sulfur atom elimination requires essentially the same activation energy.

3.3. Energy barriers comparisons

Table 5 resumes and compares the energy barriers of the various reaction channels for the subsequent reactions of S_3O_2 with those of S_4O_2. Overall, the results show that analogous reactions exhibit very similar energy barriers in both systems.

The upper part of Table 5 corresponds to the oxygen attack at the terminal sulfur while the lower part considers attack of oxygen at the inner sulfur atom.

The only notable difference is observed for the ipso addition of O_2 at the inner sulfur, where the barrier in the longer chain (S_4) is lower by approximately 13 kcal mol^{-1} compared with S_3. These comparisons, resumed in Table 5, indicate that, for structurally analogous reactions, the calculated energy barriers are consistent across different chain lengths. This observation supports the important conclusion that reaction rate parameters derived for S_3O_2 and S_4O_2 can be reasonably extended to larger sulfur–oxygen systems such as S_5O_2, S_6O_2, S_7O_2 and S_8O_2.

3.4. Kinetic calculations for $^1S_2 + {}^3O_2$ and $^1S_4 + {}^3O_2$

The reaction rate coefficients of the reactions for the reaction systems $^1S_2 + {}^3O_2$ and $^1S_4 + {}^3O_2$ were estimated using the ThermKin code [25] and are listed in Table 6, Table 7, Table 8 and Table 9 in the modified Arrhenius form,

$$k = A \cdot T^n exp(-E_A/RT)$$

Table 5. Comparison of energy barriers for the reaction channels of the $S_4 + O_2$ and $S_3 + O_2$ reaction systems.

Type of reactions	S_3O_2 (kcal mol^{-1})	S_4O_2 (kcal mol^{-1})
Attack of O_2 at the terminal sulfur atom		
O-O bond dissociation	21.0	27.2
Ring closure: 3-membered ring formation	20.8	24.5
Ring closure: 4-membered ring formation	48.5	50.0
Ring closure: 5-membered ring formation	40.6	40.8
S – S terminal sulfur bond scission	22.	24.7
S – SOO bond dissociation	11.1	17.0
Attack of O_2 at the inner sulfur atom		
O-O bond dissociation	27.1	31.9
Ring closure: 3-membered ring formation	**34.4**	**21.4**
Ring closure: 4-membered ring formation	35.3	37.
S – S terminal sulfur bond scission	32.0	31.5 /31.2
$S_3 + O_2 \rightarrow S_2O_2 + S$	67.5	–
$S_4 + O_2 \rightarrow S_3O_2 + S$	–	67.2

Table 6. Calculated input parameters[a] for the reactions used in QRRK calculations: Attack of O_2 at terminal sulfur atom of S_3.

No	Reactions	A	*n*	E_A (kcal mol^{-1})
	$^1S_3 + {}^3O_2 \rightarrow {}^1S_3O_2 \rightarrow$ Products			
1	$^1S_3 + {}^3O_2 \rightarrow {}^1S_3O_2$	3.42E + 05	1.59	26.86
	Channel-1			
2	$^1S_3O_2 \rightarrow {}^1S_3O + {}^1O$	1.77E + 12	0.52	21.33
3	$^1S_3O \rightarrow {}^1S_2O + {}^3S$	3.32E + 12	0.10	31.24
4	$^1S_3O \rightarrow {}^3S_2 + {}^3SO$	6.90E + 14	−.079	8.86
	Channel-2			
5	$^1S_3O_2 \rightarrow {}^3S_2 + {}^1SOO$	3.03E + 15	−1.05	12.31
	Channel-3			
6	$^1S_3O_2 \rightarrow {}^3S_2SO_2$	1.67E + 14	−0.89	21.96
7	$^3S_2SO_2 \rightarrow {}^3S_2 + {}^1SO_2$	8.44E + 11	0.53	−0.044
8	$^3S_2SO_2 \rightarrow {}^3S + {}^1SSO_2$	5.73E + 12	0.084	21.98
9	$SSO_2 \rightarrow {}^3S + {}^1SO_2$	2.31E + 13	0.26	53.98
	Channel-4			
10	$^3S_3O_2 \rightarrow {}^3SYS_2O_2$	1.82E + 14	−0.81	49.53
11	$^3SYS_2O_2 \rightarrow {}^1SSOSO$	5.25E + 15	−0.65	27.35
12	$^1SSOSO \rightarrow {}^1S_2O + {}^3SO$	4.42E + 15	−1.11	17.16
13	$^1SSOSO \rightarrow {}^3S + {}^1OSSO$	2.88E + 15	−0.84	24.44
	Channel-5			
14	$^3S_3O_2 \rightarrow {}^1YS_3O_2$	2.80E + 14	−1.02	41.75
15	$^3S_3O_2 \rightarrow {}^3OS_3O$	6.08E + 10	0.52	25.52
16	$^3OS_3O \rightarrow {}^3S_3O_2$	1.91E + 09	0.62	94.46
17	$^1YS_3O_2 \rightarrow {}^3OS_3O$	8.59E + 12	−0.03	−0.76
18	$^3OS_3O \rightarrow {}^1S_2O + {}^3SO$	2.81E + 12	−0.28	3.56
19	$^1YS_3O_2 \rightarrow {}^1S_2O + {}^3SO$	4.39E + 13	−0.10	19.62
	Channel-6			
20	$^3S_3O_2 \rightarrow {}^3S + {}^1S_2O_2$	4.52E + 15	−1.07	23.22

[a]The units of *A* factors and rate constants, k, are s^{-1} for unimolecular reactions and cm^3 mol^{-1} s^{-1} for bimolecular reactions. ^1X = singlet, ^3X = triplet.

ThermKin determines the forward rate constants, k(T), based on the canonical transition state theory (CTST). The modified Arrhenius parameters are determined from regression analysis with application of the principle of least squares. CTST describes the forward rate constant from reactant to the transition state (TS) as a function of the equilibrium between

Table 7. Calculated input parameters[a] for the reactions used in QRRK calculations: Attack of O_2 at the inner sulfur atom of S_3.

No	Reactions	A	*n*	E_A (kcal mol^{-1})
	$^1S_3 + {}^3O_2 \rightarrow$ iso$-{}^1S_3O_2 \rightarrow$ Products			
1	$^1S_3 + {}^3O_2 \rightarrow$ iso-$^1S_3O_2$	1.97E + 08	0.64	61.23
2	$^1S_3 + {}^3O_2 \rightarrow {}^1S_2O_2 + {}^3S$	2.18E + 06	1.67	67.53
	Channel-1			
3	iso-$^1S_3O_2 \rightarrow$ iso-$^1S_3O + {}^3O$	2.57E + 09	1.68	26.88
4	iso-$^1S_3O \rightarrow {}^3S + {}^1S_2O$	1.28E + 16	−0.90	34.10
	Channel-2			
5	iso-$^1S_3O_2 \rightarrow {}^3SYS_2O_2$	1.72E + 13	0.09	35.92
	Channel-3			
6	iso-$^1S_3O_2 \rightarrow {}^1SYSO_2S$	1.73E + 12	0.28	34.99
7	$^1SYSO_2S \rightarrow {}^3S + {}^1SSO_2$	1.10E + 14	0.23	50.19
	Channel-4			
8	iso-$^1S_3O_2 \rightarrow {}^3S + {}^1S_2O_2$	9.42E + 12	0.14	32.64

[a]The units of *A* factors and rate constants k are s^{-1} for unimolecular reactions and cm^3 mol^{-1} sec^{-1} for bimolecular reactions. ^1X = singlet, ^3X = triplet.

Table 8. Calculated input parameters[a] for the reactions used in QRRK calculations: Attack of O_2 at the terminal sulfur atom of S_4.

No	Reactions	A	*n*	E_A (kcal mol^{-1})
	$^1S_4 + {}^3O_2 \rightarrow {}^3S_4O_2 \rightarrow$ Products			
1	$^1S_4 + {}^3O_2 \rightarrow {}^3S_4O_2$	8.19E + 04	1.67	37.34
	Channel-1			
2	$^3S_4O_2 \rightarrow {}^3S_4O + {}^3O$	1.22E + 10	1.19	27.19
3	$^3S_4O \rightarrow {}^3S + {}^1S_3O$	6.20E + 10	1.11	24.28
4	$^3S_4O \rightarrow {}^2S_2 + {}^1S_2O$	3.81E + 09	2.04	1.87
5	$^3S_4O \rightarrow {}^1S_3 + {}^3SO$	8.92E + 08	2.44	22.19
	Channel-2			
6	$^3S_4O_2 \rightarrow {}^1S_2SOSO$	1.17E + 10	0.77	50.3
7	$^1S_2SOSO \rightarrow {}^1S_3O + {}^3SO$	2.81E + 16	−0.85	38.70
8	$^1S_2SOSO \rightarrow {}^1SSOSO + {}^3S$	8.52E + 13	0.13	52.97
9	$^1S_2SOSO \rightarrow {}^3S_2 + {}^1OSSO$	3.30E + 15	−0.72	16.12
	Channel-3			
10	$^3S_4O_2 \rightarrow {}^3S_3SO_2$	5.57E + 16	−1.22	26.8
11	$^3S_3SO_2 \rightarrow {}^1S_3 + {}^1SO_2$	3.79E + 13	0.17	−1.12
12	$^3S_3SO_2 \rightarrow {}^3S_2 + {}^1SSO_2$	3.56E + 11	0.24	1.84
13	$^3S_3SO_2 \rightarrow {}^3S + {}^3S_2SO_2$	1.47E + 11	0.26	22.76
	Channel-4			
14	$^3S_4O_2 \rightarrow {}^3YS_4O_2$	1.48E + 09	1.20	26.51
15	$^3YS_4O_2 \rightarrow {}^3OS_4O$	1.85E + 11	−0.53	−37.81
16	$^3OS_4O \rightarrow 2{}^1S_2O$	2.23E + 09	1.28	4.30
17	$^3OS_4O \rightarrow {}^1S_3O + {}^3SO$	6.99E + 09	1.24077	7.52
18	$^3OS_4O \rightarrow 2{}^1S_2O$	3.82E + 10	0.33	58.47
	Channel-5			
19	$^3S_4O_2 \rightarrow {}^1SYS_3O_2$	2.63E + 09	1.013	40.72
20	$^1SYS_3O_2 \rightarrow {}^3S + YS_3O_2$	3.01E + 14	−0.48	42.35
	Channel-6			
21	$^3S_4O_2 \rightarrow {}^3S_3 + {}^1SOO$	1.13E + 10	0.99	17.00
	Channel-7			
22	$^3S_4O_2 \rightarrow {}^3S_2 + {}^1SSO_2$	8.76E + 09	1.06	33.09
	Channel-8			
23	$^3S_4O_2 \rightarrow {}^3S + {}^3S_3O_2$	2.40E + 10	0.94	24.72

[a]The units of *A* factors and rate constants k are s^{-1} for unimolecular reactions and cm^3 mol^{-1} sec^{-1} for bimolecular reactions. ^1X = singlet, ^3X = triplet.

Table 9. Calculated input parameters[a] for the reactions used in QRRK calculations: Attack of O_2 at the inner sulfur atom of S_4.

No	Reactions	A	*n*	E_A (kcal mol^{-1})
	$^1S_4 + {}^3O_2 \rightarrow$ iso-$^3S_4O_2 \rightarrow$ Products			
1	$^1S_4 + {}^3O_2 \rightarrow$ iso-$^3S_4O_2$	4.96E + 08	0.53	41.78
2	$^1S_4 + {}^3O_2 \rightarrow {}^1S_3O_2 + {}^3S$	1.77E + 08	0.67	68.99
3	$^1S_4 + {}^3O_2 \rightarrow {}^1S_2O_2 + {}^3S_2$	2.11E + 09	0.63	52.74
	Channel-1			
4	iso-$^3S_4O_2 \rightarrow$ iso-$^3S_4O + {}^3O$	9.06E + 09	1.33	31.80
5	iso-$^3S_4O \rightarrow {}^2S_2O + {}^3S_2$	9.58E + 15	−1.10	3.65
6	iso-$^3S_4O \rightarrow {}^1S_3O + {}^3S$	4.42E + 15	−0.92	21.99
7	Iso-$^3S_4O \rightarrow$ iso-$^1S_3O + {}^3S$	9.71E + 13	−0.08	44.55
	Channel-2			
8	iso-$^3S_4O_2 \rightarrow {}^1SYS_2O_2S$	9.57E + 13	−0.96	56.97
9	$^1SYS_2O_2S \rightarrow {}^1SSOSOS$	6.94E + 12	−0.05	14.23
10	$^1SSOSOS \rightarrow {}^3S + {}^3SSOSO$	1.27E + 15	−0.92	28.59
11	$^3SSOSO \rightarrow {}^3S + {}^1OSSO$	1.00E + 15	−1.01	31.92
12	$SSOSO \rightarrow {}^1S_2O + {}^3SO$	5.19E + 14	−1.03	0.054
	Channel-3			
13	iso-$^3S_4O_2 \rightarrow SYS_3O_2$	2.06E + 12	−0.24	31.12
	Channel-4			
14	iso-$^3S_4O_2 \rightarrow S_2YS_2O_2$	1.53E + 14	−1.20	38.29
	Channel-5			
15	iso-$^3S_4O_2 \rightarrow {}^1S_2SO_2S$	3.32E + 13	−0.79	22.57
16	$^3S_2SO_2S = {}^3S_2 + {}^1SSO2$	2.71E + 11	1.03	−5.44
	Channel-6			
17	iso-$^3S_4O_2 \rightarrow {}^3S_2 + {}^1SSO_2$	3.30E + 11	−0.17	24.98
	Channel-7			
18	iso-$^3S_4O_2 \rightarrow {}^3S +$ iso-$^3S_3O_2$	4.02E + 12	−0.16	32.23
	Channel-8			
19	iso-$^3S_4O_2 \rightarrow {}^3S + {}^1S_3O_2$	6.84E + 14	−0.92	32.47

[a][a]The units of *A* factors and rate constants k are s^{-1} for unimolecular reactions and cm^3 mol^{-1} sec^{-1} for bimolecular reactions. ^1X = singlet, ^3X = triplet.

reactant and TS. For the calculations thermodynamic properties of reactants and transition states are prerequisite. ThermKin requires the thermodynamic properties to be in the NASA polynomial format.

The reaction rate parameters are calculated for the reactions involving the attack of O_2 at each S_3 and S_4. For both compounds attack at the terminal and the inner sulfur atom of both S_3 and S_4 are possible. The reaction rate coefficients are estimated for the following systems:

$^1S_3 + {}^3O_2 \rightarrow {}^1S_3O_2 \rightarrow$ Products

$^1S_3 + {}^3O_2 \rightarrow$ iso$-{}^1S_3O_2 \rightarrow$ Products

as well as for the S_4 system:

$^1S_4 + {}^3O_2 \rightarrow {}^3S_4O_2 \rightarrow$ Products

$^1S_4 + {}^3O_2 \rightarrow$ iso$-{}^3S_4O_2 \rightarrow$ Products.

In order to compare the reactions involved in the oxidation of S_3 and S_4, multi-channel multi-frequency QRRK [29,30] calculations are performed for *k(E)* with master equation analysis (CHEMASTER code] [31,25]) for the $S_3 + O_2$ and $S_4 + O_2$ systems. The analysis gives estimates of the rate coefficients k(T) for the stabilization of the formed adducts and reaction products of the successive reactions at different temperatures and pressures. The rate coefficients calculated with ThermKin serve as input for the QRRK analysis. Figure 14 compares the calculated rate constants as function of temperature calculated for the same

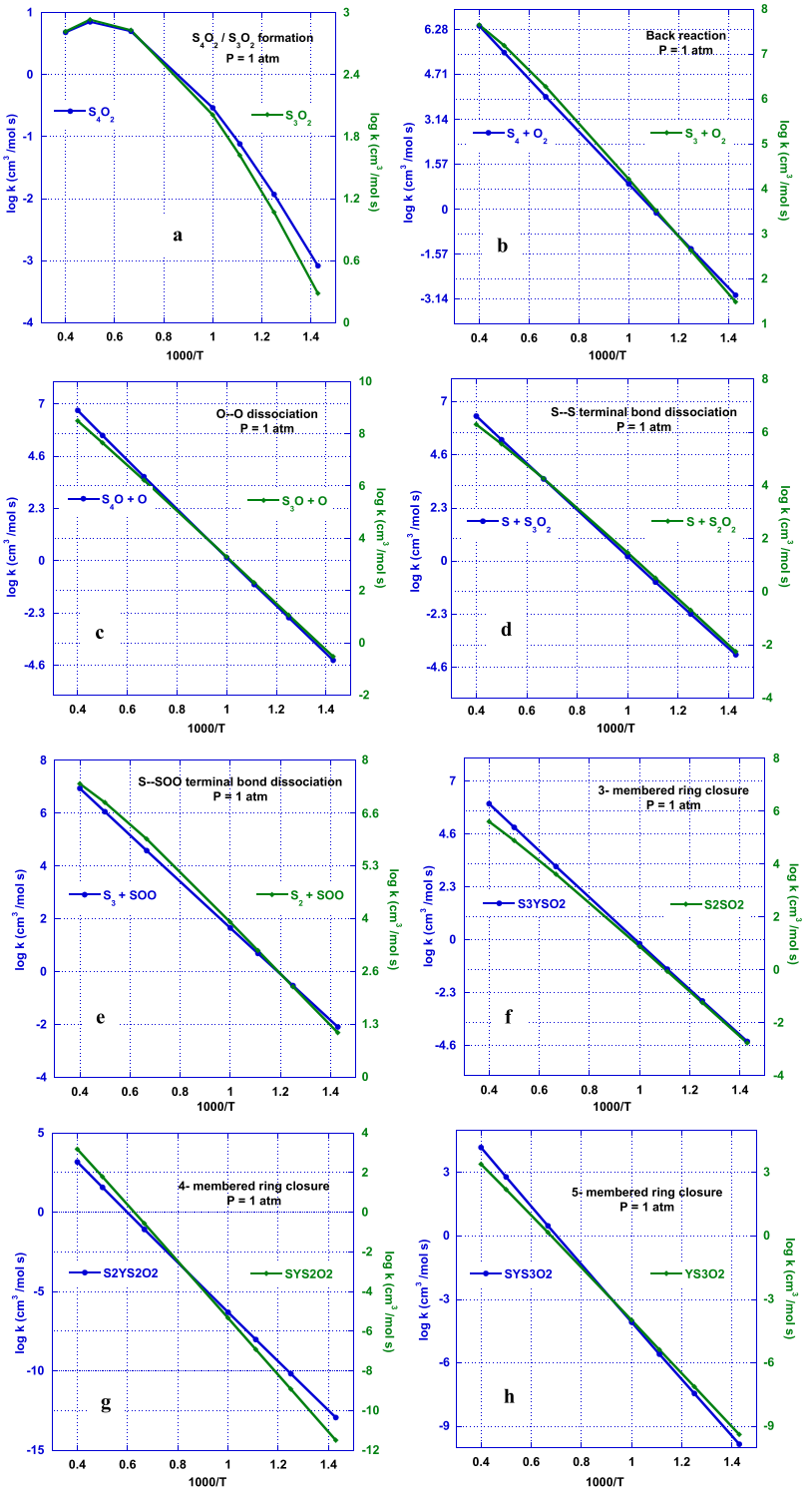

Figure 15. Attack of O_2 at terminal sulfur of S_3 and S_4: (a) Comparison of S_3O_2/S_4O_2 formation; (b) comparison of back reaction to $S_3 + O_2/S_4 + O_2$; (c) comparison of O-O bond scission in S_3O_2/S_4O_2; (d) comparison of S-S bond scission in S_3O_2/S_4O_2; (e) comparison of S-SOO bond scission in S_3O_2/S_4O_2; (f) comparison of 3-membered-ring closure; (g) comparison of 4-membered-ring closure; (h) comparison of 5-membered-ring closure.

type of reactions of the $S_3 + O_2$ and $S_4 + O_2$ systems (attack of O_2 at the terminal sulfur atom), e.g. Figure 15c illustrates the O-O bond scission for S_3 and S_4 showing the same slope for both cases. For all reactions similarities between $S_3 + O_2$ and $S_4 + O_2$ systems can be recognized.

The reactions listed in Table 6, Table 7, 8 and Table 9 can be incorporated into the combustion mechanism of the $S_2 + O_2$ system, as developed in previous work [16], along with relevant data from literature, e.g. [28,33]. Integration of these reactions contributes to constructing a detailed reaction mechanism that can be used to evaluate key combustion properties of sulfur, including auto-ignition times, flame propagation velocities, and other kinetic characteristics relevant to sulfur oxidation processes

4. Conclusions

The present study investigates plausible reaction pathways arising from the oxidation of the small sulfur clusters $^1S_3$ and $^1S_4$, extending our previous work on the $^3S_2 + {}^3O_2$ reaction system. Understanding the oxidation of small sulfur species is crucial, as these reactions play a key role in sulfur combustion and atmospheric chemistry, influencing both pollutant formation and energy release. In these systems, molecular oxygen ($^3O_2$) can interact with both terminal and internal sulfur atoms of $^1S_3$ and $^1S_4$.

Thermochemical properties were performed with the help of high-level ab initio quantum chemical calculations at CBS-QB3, G3, and G4 levels. These methods provide reliable structural and energetic information for all intermediates and transition state structures involved in both reaction systems.

For the $^1S_3 + O_2$ system, addition of O_2 to the terminal sulfur atom produces the intermediate $^1S_3O_2$, while addition to the internal sulfur atom yields iso$-{}^1S_3O_2$. Similarly, in the $^1S_4 + O_2$ system, O_2 addition to the terminal sulfur leads to $^1S_4O_2$, and addition to an internal sulfur atom forms iso$-{}^3S_4O_2$. These primary intermediates undergo a series of subsequent reactions, including bond rearrangements, dissociation and O–S migrations, lead to the formation of the final products ^1S_2O, ^3SO, ^3S, $^3S_2$, and $^1SO_2$.

This study also presents new reaction rate coefficients for the pathways initiated by O_2 addition to S_3 and S_4. The calculated rates for the formation of primary intermediates show consistent trends among analogous reaction types. This consistency is particularly valuable, as it allows the extrapolation of kinetic data to larger sulfur species, potentially up to S_8, which are relevant in combustion and atmospheric processes. Consequently, the results of this study provide a solid basis for extending existing detailed reaction mechanisms for sulfur combustion.

The data generated in this study can be directly applied to extend existing detailed reaction mechanisms for sulfur combustion, providing kinetic information for larger systems.

Acknowledgements

The results presented in this study have been obtained within the framework of the European research project SULPHURREAL. This project has received funding from the European Union's European Innovation Council and SMEs Executive Agency (EISMEA) program under grant agreement no 101115538.

Author contributions

CRediT: **Nadia Sebbar:** Writing – original draft, Writing – review & editing; **Henning Bockhorn:** Supervision, Validation; **Dimosthenis Trimis:** Project administration

Disclosure statement

No potential conflict of interest was reported by the author(s).

Funding

This project has received funding from the European Union's European Innovation Council and SMEs Executive Agency (EISMEA) program under grant agreement no 101115538.

References

[1] Clark PD, Dowling ND. Capture of solar energy using elemental sulfur. J Sulfur Chem. 2004;25:7–11. doi:10.1080/17415990410001661267
[2] Zhang F, Kurjata M, Sebbar N, et al. Numerical study on flame stabilization and NOx formation in a novel burner system for sulfur combustion. Energy Fuels. 2022;36:4094–4106. doi:10.1021/acs.energyfuels.1c04007
[3] Abumounshar NM, Ibrahim S, Raj S. A detailed reaction mechanism for elemental sulphur combustion in the furnace of sulphuric acid plants. Can J Chem Eng. 2021: 1–11. doi:10.1002/cjce.24185
[4] Giménez-López J, Martínez M, Millera A, et al. SO_2 effects on CO oxidation in a CO_2 atmosphere: characteristic of oxy-fuel conditions. Combust Flame. 2011;158:48–56. doi:10.1016/j.combustflame.2010.07.017
[5] Zeng Z, Altarawneh M, Oluwoye I, et al. Inhibition and promotion of pyrolysis by hydrogen sulfide (H2S) and sulfanyl radical (SH). J Phys Chem A. 2016;120:8941–8948. doi:10.1021/acs.jpca.6b09357
[6] Glarborg P, Marshall P. Oxidation of reduced sulfur species: carbonyl sulfide. Int J Chem Kinet. 2013;45:429–439. doi:10.1002/kin.20778
[7] Song Y, Hashemi H, Christensen JM, et al. An exploratory flow reactor study of H_2S oxidation at 30–100 Bar. Int J Chem Kinet. 2017;49:37–52. doi:10.1002/kin.21055
[8] Alzueta MU, Bilbao R, Glarborg P. Inhibition and sensitization of fuel oxidation by SO_2. Combust Flame. 2001;127:2234–2251. doi:10.1016/S0010-2180(01)00325-X
[9] Du S, Germann TC, Francisco JS, et al. The kinetics study of the S + S2 → S3 reaction by the chaperone mechanism. J Chem Phys. 2011;134:154508), doi:10.1063/1.3572226
[10] Francisco S. High-level ab initio studies of the structure: vibrational spectra, and energetics of S3. J Chem Phys. 2005;123:054302), doi:10.1063/1.1979474
[11] Matus MH, Dixon DA, Peterson KA, et al. Coupled-cluster study of the electronic structure and energetics of tetrasulfur S4. J Chem Phys. 2007;127:174305), doi:10.1063/1.2774973
[12] Wong MW, Steudel R. Structure and spectra of tetrasulfur S4 – an ab initio MO study. Chem Phys Letters. 2003;379:162–169. doi:10.1016/j.cplett.2003.08.026
[13] McCarthy MC MC, Thorwirth S S, Gottlieb CA CA, et al. Tetrasulfur, S4: rotational spectrum: interchange tunneling, and geometrical structure. J Chem Phys. 2004;121:632–635. doi:10.1063/1.1769372
[14] Sebbar N, Bozzelli JW, Bockhorn H, et al. A thermochemical study on the primary oxidation of sulfur. Combust Sci Technol. 2019;191:163–177. doi:10.1080/00102202.2018.1455134
[15] Glarborg P, Kubel D, Dam-Johansen K, et al. Impact of SO_2 and NO an CO oxidation under post-flame conditiins. Int J Chem Kinet. 1996;28:773–790. doi:10.1002/(SICI)1097-4601(1996)28:10<773::AID-KIN8>3.0.CO;2-K

[16] Sebbar N, Bockhorn H, Bozzelli JW, et al. Computational investigation of the isomers formed from the reaction $S_2 + O_2$. J Sulfur Chem. 2025;25:416–434. doi:10.1080/17415993.2025.2473740
[17] Sebbar N, Bockhorn H, Trimis D. Computational study of the dissociation reactions of S8 and the resulting fragments S7, S6, S5, S4, and S3: Thermodynamic data and kinetics. 12th European Combustion Symposium 2025, Edinburgh.
[18] Sebbar N, Bockhorn H, Trimis D. Decomposition of S8 and its fragments through O_2 oxidation: Thermochemistry and reaction mechanism. 13th Mediterraneum combustion symposium 2025, Corfu.
[19] Frisch MJ, Trucks GW, Schlegel HB, et al. Gaussian 09, revision A02, Wallingford CT, 2016.
[20] Montgomery JA Jr, Frisch MJ, Ochterski JW, et al. A complete basis set model chemistry. VI: use of density functional geometries and frequencies. J Chem Phys. 1999;110:2822–2827.
[21] Curtiss LA, Raghavachari K, Redfern PC, et al. Gaussian-3 (G3) theory for molecules containing first and second-row atoms. J Chem Phys. 1998;109:7764–7776. doi:10.1063/1.477422
[22] Curtiss LA, Redfern PC, Raghavachari K. Gaussian-4 theory. J Chem Phys. 2007;126:0841081–08410812.
[23] Martin JML, De Oliveira D. Towards standard methods for benchmark quality ab initio thermochemistry – W1 and W2 theory. J Chem Phys. 1999;111:1843–1856. doi:10.1063/1.479454
[24] Goodarzi M, Vahedpour M, Nazari F. Theoretical study on the atmospheric formation of cis and trans-OSSO complexes. Chem Phys Lett. 2010;494:315–322. doi:10.1016/j.cplett.2010.06.001
[25] Sheng C. Elementary, pressure dependent model for combustion of C1, C2 and nitrogen containing hydrocarbons: Operation of a pilot scale incinerator and model comparison. Dissertations 518 (2002), https://digitalcommons.njit.edu/dissertations/518.
[26] Cox JD, Wagman DD, Medvedev VA. CODATA key values for thermodynamics. New York: Hemisphere Publishing Corp.; 1984.
[27] Chase MW Jr. NIST-JANAF thermochemical tables, Fourth Edition, J. Phys. Chem. Ref. Data, Monograph 9, 1998, 1-1951.
[28] McBride BJ, Zehe MJ, Gordon S. NASA glenn coefficients for calculating thermodynamic properties of individual species. NASA/TP—2002-211556. Cleveland (OH): Glenn Research Center; 2002.
[29] Chang AY, Bozzelli JW, Dean AM. Kinetic analysis of complex chemical activation and unimolecular dissociation reactions using QRRK theory and the modified strong collision approximation. Z Phys Chem. 2000;214:1533–1568. doi:10.1524/zpch.2000.214.11.1533
[30] Sheng C, Bozzelli JW, Dean AM, et al. Detailed kinetics and thermochemistry of $C_2H_5 + O_2$: reaction kinetics of the chemically-activated and stabilized $CH_3CH_2OO\bullet$ adduct. J PhysChem A. 2002;106:7276–7293.
[31] Dean AM, Bozzelli JW, Ritter ER. CHEMACT: A computer code to estimate rate constants for chemically-activated reactions. Combust Sci Technol. 1991;80:63–85. doi:10.1080/00102209108951777
[32] Hughes KJ, Blitz MA, Pilling MJ, et al. Proc Combust Inst. 2002;29:2431–2437. doi:10.1016/S1540-7489(02)80296-6
[33] Sebbar N, Zirwes T, Habisreuther P, et al. S_2 + air combustion: reaction kinetics, flame structure, and laminar flame behavior energy. Fuels. 2018;32:10184–10193. doi:10.1021/acs.energyfuels.8b01019